Quaternary Science Reviews 30 (2011) 2069–2090

Contents lists available at ScienceDirect

Quaternary Science Reviews

journal homepage: www.elsevier.com/locate/quascirev

Old Crow tephra across eastern Beringia: a single cataclysmic eruption at the close of Marine Isotope Stage 6

S.J. Preece [a], N.J.G. Pearce [b], J.A. Westgate [a,*], D.G. Froese [c], B.J.L. Jensen [c], W.T. Perkins [b]

[a] Department of Geology, University of Toronto, Toronto, ON M5S 3B1, Canada
[b] Institute of Geography and Earth Science, Aberystwyth University, Wales SY23 3DB, UK
[c] Department of Earth and Atmospheric Sciences, University of Alberta, Edmonton, AB T6G 2E3, Canada

ARTICLE INFO

Article history:
Received 21 August 2009
Received in revised form
31 March 2010
Accepted 21 April 2010
Available online 31 May 2010

ABSTRACT

Old Crow tephra is the largest and most widespread Quaternary eruption presently known in eastern Beringia. Its major- and trace-element geochemistry, Fe-Ti oxides, and stratigraphic and paleoecological context indicate that it is the result of a single cataclysmic eruption. The proximal region may well have experienced tephra fallout from small eruptions just prior to or after the Old Crow event, but there is no evidence to indicate that the distal area was affected. We recalculate the glass fission-track age at 124 ± 10 ka, which, coupled with stratigraphic and paleoenvironmental reconstructions, indicates that deposition occurred prior to development of the last interglacial boreal forest, which suggests a latest Marine Isotope Stage (MIS) 6 age. The bulk tephra volume erupted is estimated by three different approaches, that are in broad agreement at $\sim 200\ km^3$, but this result must be considered as tentative given the poor controls on definition of isopachs over such a large area. The source caldera, although presently unrecognized, is located in the eastern Aleutian arc, possibly at or near the Emmons Lake volcanic center.

1. Introduction

Old Crow tephra (OCt) is widely distributed across eastern Beringia (Fig. 1) and is found in a variety of depositional environments (Table 1). It has an age of about 130 ka (Péwé et al., 2009) and serves as an excellent stratigraphic marker for the last interglacial deposits in this region (Hamilton and Brigham-Grette, 1991). At sites in southwestern Alaska and southern Yukon it is closely associated with glacial drift sheets and provides age constraints on glacial advances (Kaufman et al., 2001a; Ward et al., 2008). However, a number of observations raise the possibility that Old Crow tephra might represent more than one volcanic eruption. For example, most OCt sites are consistent with deposition at a time when conditions were colder than those of today, but a few suggest warmer conditions (Hamilton and Brigham-Grette, 1991; Muhs et al., 2001). Silt/tephra couplets occur at site 10 (Fig. 1) along the Koyukuk River, the tephra is stratified at site 12, near Halfway House, Alaska, and at Eva II near Fairbanks (site 13), OCt is found in very different types of sediment across the exposure (Muhs et al., 2001). In this study, we attempt to resolve this uncertainty. Is OCt related to one large-magnitude eruption or several?

Provided tephra beds are characterized in detail, including criteria such as stratigraphy, age, petrography, and chemical attributes of glass shards and/or mineral phases (Westgate and Gorton, 1981; Alloway et al., 2007), repeated eruptions from a single volcanic complex can be recognized. Tephra associated with each eruption should have different glass shard and/or mineral compositions because magma chemistry changes over time through processes such as crystallisation, assimilation of country rock, recharge by new injections of magma, and resulting changes in parameters such as temperature and oxygen fugacity (e.g. O'Hara and Mathews, 1981). These differences may be subtle and require different chemical data sets to detect. For example, detailed studies of multiple tephra horizons from individual volcanic complexes show variations in glass shard and/or mineral compositions, and in geothermometry estimates from Fe-Ti oxide pairs. In the Alaska/Yukon region, the northern and eastern lobes of White River Ash have nearly identical compositions for their glass shards, but have readily distinguishable Fe-Ti oxide compositions and geothermometry estimates (Lerbekmo et al., 1975; Froese and Jensen,

* Corresponding author. Tel.: +1 416 488 6838; fax: +1 416 978 3938.
E-mail addresses: sjpreece@rogers.com (S.J. Preece), njp@aber.ac.uk (N.J.G. Pearce), westgate@geology.utoronto.ca (J.A. Westgate), duane.froese@ualberta.ca (D.G. Froese), bjjensen@ualberta.ca (B.J.L. Jensen), wwp@aber.ac.uk (W.T. Perkins).

0277-3791/$ – see front matter © 2010 Elsevier Ltd. All rights reserved.
doi:10.1016/j.quascirev.2010.04.020

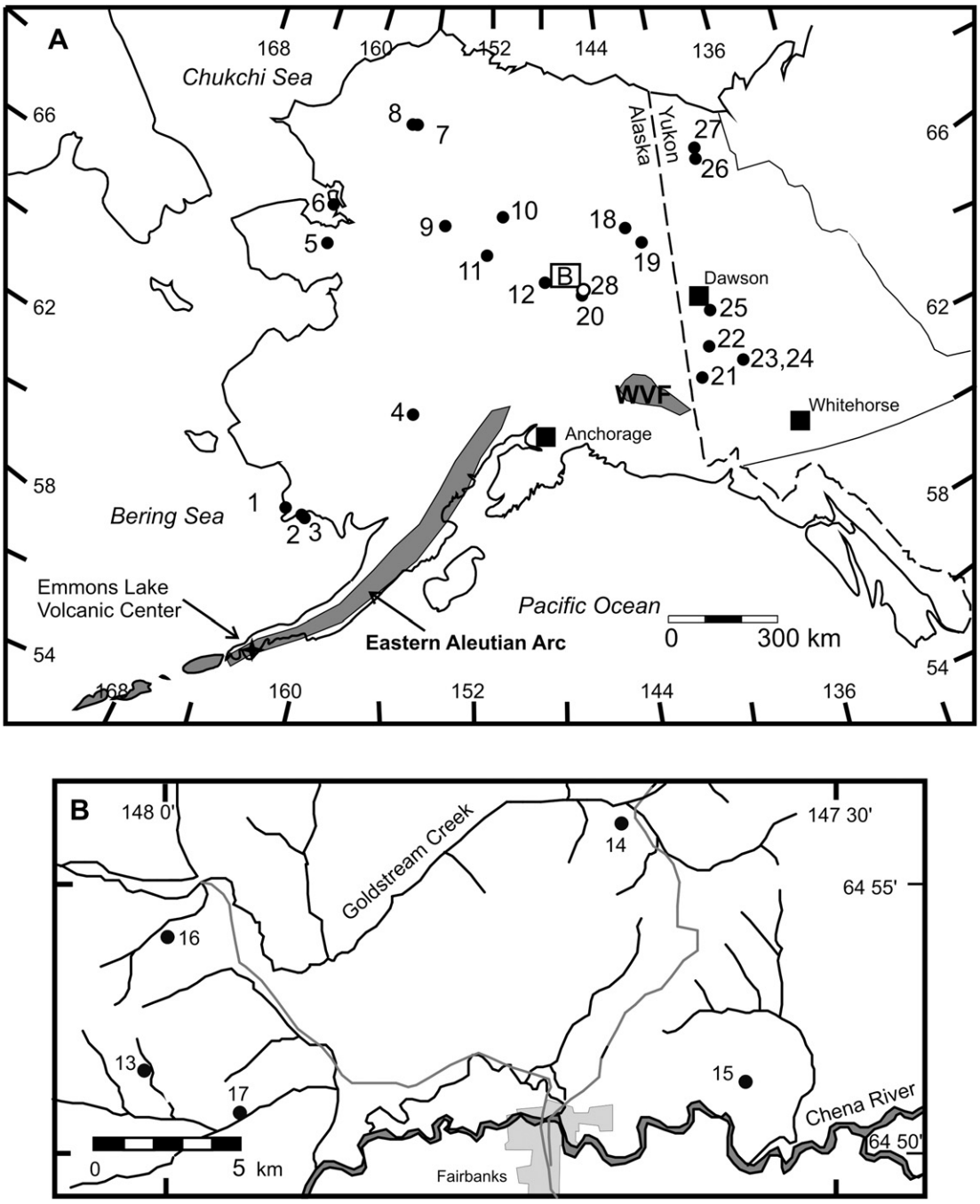

Fig. 1. A. Map showing locations of Old Crow tephra samples. B. Map of Old Crow tephra samples in the Fairbanks area. Sample sites are as follows: 1. Goodnews Bay, 2. Togiak Bay, 3. Hagemeister Island, 4. Holtina, 5. Imruk Lake, 6. Baldwin Peninsula, 7. Noatak River, NK26B, 8. Noatak River, NK29A, 9. Hogatza Mine, 10. Koyukuk River, Ky-11, 11. Palisades, Yukon River, 12. Halfway House, 13. Eva II, 14. West Dawson, 15. Birch Hill, 16. Sheep Creek Valley, 17. Gold Hill, 18. Birch Creek, 19. Chester Bluff, 20. Mile 293 Richardson Highway, 21. Mirror Creek, 22. Thistle, 23. Caribou Creek 1, 24. Caribou Creek 2, 25. Klondike, 26. UT 1 type locality at Chi'jee's Bluff, 27. Old Crow Basin, 28. Begét and Keskinen (2003) locality at Moose Creek (symbol "o"), not analyzed in this study. See Table 1 for additional details. WVF is the Wrangell volcanic field.

2005). Sheep Creek tephra beds (F, K, A, C, CC) have very similar compositions, but can be separated using K_2O and trace-element concentrations in their glass shards (Westgate et al., 2008). Elsewhere, widespread tephra beds from Yellowstone have very similar major-element compositions of their glass shards, but can easily be identified using their trace-element content (Pearce et al., 2004). In New Zealand, the major-element composition of both glass shards and Fe-Ti oxides combined with geothermometry estimates have been extensively used to identify tephra beds from different volcanic complexes and multiple eruptions from individual volcanic complexes (Shane, 1998; Smith et al., 2005). Unfortunately, the published chemical data for OCt derive from several different methods and calibrations, and, although these data are in broad agreement, they cannot document small variations that might be present in multiple eruptions (Westgate et al., 1985; Preece et al., 1999; Begét and Keskinen, 2003). In this study, we reanalyze OCt samples from 27 sites using consistent methodology and calibration for glass shard, titano-magnetite, and ilmenite compositions and estimate the temperature and oxygen fugacity from the Fe-Ti oxide data. Statistical and graphical methods are used to evaluate

Table 1
Location and stratigraphy of Old Crow tephra samples.

Site number	Sample number	Site name	Latitude (N) Longitude (W)	Thickness (cm)	Stratigraphy
1	UT1407	Goodnews Bay, DK95-25	58° 46.977′ 161° 11.021′	Few mm	OCt occurs as reworked pumiceous lapilli forming small-scale cross-sets in well-sorted, fine sand of a composite ridge that is part of the early Wisconsin drift sheet (D. Kaufman et al., 2001a; D. Kaufman, written comm. 31/10/2008). Located 25.5 m above sea level.
2	UT1434	Togiak Bay, WM97-61	58° 47.38′ 161° 10.75′	40	A faulted and folded tephra bed within glaciotectonized sediments underlying drift deposits (Kaufman et al., 2001a; Kaufman, written comm. 25/7/1997).
3	UT1577	Hagemeister Island, WM98-05	58° 42.3′ 161° 02.2′	15	Tephra bed is deformed and faulted within glaciotectonized sediments (Kaufman et al., 2001a; W. Manley, pers. comm. 23/12/1998). Located 7.1 m above sea level in a coastal wave-cut exposure.
4	UT613	Holitna	61° 14.28′ 157° 7.92′	35 to 45	Tephra in periglacial fining-upward sand and silt aeolian unit that overlies distal outwash deposit and underlies a reworked, slightly organic to peaty silt deposit. It is weakly laminated to massively bedded within a massive loess near top of eolian unit. Ice-wedge casts are located at the top of aeolian unit and locally deform OCt (Waythomas et al., 1993).
5	UT371	Imruk Lake	65° 37′ 163° 11′	10	Occurs at 525–535 cm depth in pollen zone G4 in Imruk Lake core V. A paleomagnetic excursion underlies OCt (Hamilton and Brigham-Grette, 1991).
6	UT976	Baldwin Peninsula	66° 40.410′ 162° 09.195′	0.5 to 1	OCt occurs as discontinuous pods in bedded clayey silt and clay near base of organic-rich silt (loess) with prominent log layers. The organic-rich silts underlie Holocene peat and thaw-lake deposits. Tephra is at 23 m on figure 13 of Hamilton and Brigham-Grette (1991). Brigham-Grette, written comm. 31/10/2008.
7	UT1714	Noatak River, NK26B	67° 55.615′ 158° 21.458′	4	Small pods of tephra within dark brown, organic-rich silt with many cobbles and some peaty patches. These flood-plain deposits fill depressions on the surface of underlying gravel (unit 5 of Elias et al., 1999) and are overlain by glaciolacustrine stony mud (unit 6 of Elias et al., 1999).
8	UT1718	Noatak River, NK29A	68° 01.445′ 158° 32.484′	3	Small pods of tephra occur over 1.1 m laterally within dark brown, organic-rich silty flood-plain deposits. Locally, the organic-rich silt is capped with a peaty bed and grey silt. Tephra is cut by an ice wedge cast and is located 16 m above river level (Elias et al., 1999)..
9	UT718	Hogatza Mine	66° 11.5′ 155° 41.5′	1 to 25	Tephra bed within loess a few centimeters above prominent peat layer with abundant Picea pollen (Hamilton and Brigham-Grette, 1991).
10	UT1833, UT1834a, UT1834b, UT1834c, UT1834d	Koyukuk, Ky-11	66° 32.5′ 152° 05′	30	OCt occurs near base of ~ 6 m of bedded silt that is overlain by a peaty bed containing pollen similar to that of today. The peat is overlain by loess. OCt is 5 cm and covered by couplets of grey silt and tephra for a combined thickness of 30 cm (Westgate et al., 1983; Hamilton and Brigham-Grette, 1991).
11	UA1124, UA1198	Palisades, Yukon River	65° 5.7′ 153° 16.7′	10	OCt is 2 to 3.5 m below woody, organic-rich silt and peat that host abundant large stumps and logs. It occurs as pods and lenses offset by centimetre-scale faults within massive, grey silt. Located 25 to 30 m above Yukon River.
12	UT815, UT896, UT897, UT898, UT899, UT900, UT901	Halfway House	64° 43.68′ 148° 26.94′	30	Thick, continuous tephra bed within the Upper Gold Hill Loess overlying basement schist and about 3 m below a laminated organic silt containing SD tephra (Preece et al., 1999; Berger, 2003). Lower 14 cm consist of four subhorizontal fining-upward layers, which are covered by 16 cm of reworked tephra.
13	UT828, UT1727, UT1730, UT1731, UT1733, UT410, UT388	Fairbanks, Eva II	64° 51.06′ 148° 0.54′	18	Pods of tephra within Upper Gold Hill Loess about 1.5 m below Eva Forest Bed (Preece et al., 1999).
14	UT420	Fairbanks, West Dawson	64° 56.64′ 147° 38.82′	n.d.	In the Upper Gold Hill Loess (Péwé et al., 2009).
15	UT1002	Fairbanks, Birch Hill	64° 51′ 147° 34′	10	Thick, continuous bed within the Upper Gold Hill Loess (Berger, 2003).
16	UA368	Fairbanks, Sheep Creek	64°54′ 148°	n.d.	In the Upper Gold Hill Loess (Péwé et al., 2009).
17	UA348	Fairbanks, Gold Hill	64° 51.48 147° 55.98′	13	In the Upper Gold Hill Loess just beneath unconformity with Goldstream Formation (Péwé et al., 2009).
18	UT543	Birch Creek	65° 49.02′ 144° 18′	15-20	Within thick section of fluvial, loessial and lacustrine sediments containing several paleosols. OCt is located between units D and E on peaty, duff layer overlying loess. About 4.5 m above OCt, in unit F, beaver-cut wood is found at base of horizontally laminated silt containing pollen indicative of conditions as warm as the Holocene (McDowell and Edwards, 2001).
19	UA1099, UA1233, UA1211	Chester Bluff	65° 20.1′ 142° 43.92	25	Tephra bed within remobilized, massive inorganic loess. An organic-rich loess up to 60 cm thick occurs 20 to 40 cm above OCt (Jensen et al., 2008).
20	UT524	Mile 293 Richardson Hwy.	64° 16.98′ 146° 19.26′	6 to 22	6 to 7 m below surface within loess-aeolian sand deposits (Péwé and Reger, 1983).
21	UA339	Mirror Creek	62° 31′ 140° 56.5′	<1.5	2 m below surface in silts overlying the Mirror Creek Till (V. Rampton, written comm., 1971).
22	UT1805, UT1816, UT1823	Thistle Creek	63° 6′ 139° 18′	1.5 to 15	Sections at Thistle Creek contain 3 organic-rich silt beds intercalated with loess. OCt occurs within loess between the 2 lowermost organic-rich silt beds (Westgate et al., 2009).
23	UA1240	Caribou Creek 1	62° 51′ 137° 12′	4 to 6	Within well-stratified sand and silt of an alluvial fan overlying Reid deglacial gravels (Ward et al., 2008).
24	UA1274	Caribou Creek 2	62° 52.2′ 137° 1.8′	2 to 3	Within sandy-silt overlying gravel (Ward et al., 2008).

(*continued on next page*)

Table 1 (*continued*)

Site number	Sample number	Site name	Latitude (N) Longitude (W)	Thickness (cm)	Stratigraphy
25	UT17	Klondike	64° 0.32′ 139° 5.15′	10	1 m long tephra bed at base of 10 m-thick muck overlying 1 m of gravel (Preece et al., 2000).
26	UT1	Ch'ijee's Bluff, Bluefish Basin	67° 28′ 139° 54′	5 to 10	OCt occurs as a layer that is disrupted and deformed adjacent to and within an ice-wedge cast in fine-grained, peaty fluvial deposits (Westgate et al., 1983). Pollen associated with OCt indicates that climate was colder than present. Approximately 3 m above OCt, pollen, plant macrofossils and insect macrofossils demonstrate climatic warming (Matthews et al., 1990).
27	UT50	Old Crow Basin locality 15	67° 51.5′ 139° 49.6′	5	Occurs in cryoturbated clayey silts,and within ice-wedge casts that are bounded above and below by lacustrine clay (Schweger and Matthews, 1985).

the compositional homogeneity of the OCt samples and compare them to compositionally similar tephra deposits in order to determine if there is evidence for more than one OCt eruption. A revised glass fission-track age estimate and a bulk volume estimate are also reported. Finally, we suggest a possible source for OCt.

2. Previous work

2.1. Stratigraphic setting

The varied stratigraphic settings of OCt in eastern Beringia are summarized in Table 1. Old Crow tephra is interbedded within fluvial deposits at its type locality at Ch'ijee's Bluff along the Porcupine River near Old Crow in northern Yukon and at two sites on the Noatak River (Fig. 1, Table 1, sites 26, 7 and 8, respectively). It is closely associated with glacial deposits at site 1 in SW Alaska and sites 23 and 24 in SW Yukon. Host sediments at Imruk Lake (site 5) and Koyukuk (site 10) are of lacustrine origin, whereas in the Old Crow Basin (sites 26, 27) OCt occurs in both fluvial and lacustrine sediments. Old Crow tephra has been found in pond deposits within a loess unit on the Baldwin Peninsula (site 6) and in glaciotectonized marine sediments at Hagemeister Island and Togiak Bay, SW Alaska (sites 2, 3). Aeolian sands form the host sediments at Holitna (site 4) and the Richardson Highway site 20. At all other localities, OCt is associated with loess or reworked loess (Table 1).

2.2. Chemical characterization

Previous studies have documented the major-element composition of glass shards in OCt by utilizing the electron microprobe, and trace-element composition of glass shards by using either one or a combination of the following methods: instrumental neutron activation, ion microprobe, solution nebulization inductively-coupled plasma-mass spectrometry (ICP-MS), and laser ablation ICP-MS (LA-ICP-MS). Analyzed samples come from locations 1, 2, 3, 4, 5, 10, 12, 13, 16, 17, 21, 25, 26, and 28 (Fig. 1; Westgate et al., 1985; Westgate, 1988; Preece et al., 1999; Preece et al., 2000; Kaufman et al., 2001b; Begét and Keskinen, 2003; Pearce et al., 2004). Additional major-element analyses of glass from OCt are reported from the Palisades site along the Yukon River (Fig. 1, site 11, Begét et al., 1991; Matheus et al., 2003), Noatak River (Fig. 1, site 7, Elias et al., 1999), Birch Hill (site 15, Péwé et al., 2009), West Dawson (site 14, Péwé et al., 2009), Chester Bluff (site 19, Jensen et al., 2008), southern Yukon (sites 23, 24, Ward et al., 2008), Thistle Creek (site 22, Westgate et al., 2009), and Eva II at Fairbanks (site 13, Muhs et al., 2001). Only trace-element data on OCt glass is reported for occurrences at sites 18 and 20 (Westgate et al., 1985). Major-element compositions of sanidine, plagioclase, pyroxene, magnetite, and ilmenite are listed in Westgate et al. (1983, 1985). No chemical data on OCt has been published for the occurrences at Baldwin Peninsula (site 6), Noatak River (site 8), and Hogatza Mine (site 9).

3. Geochemical analytical methods

3.1. Sample preparation

Tephra samples were wet sieved into >0.25 mm, 0.25–0.125 mm, 0.125–0.105 mm, 0.105–0.0625 mm and <0.0625 mm fractions and inspected for glass shards, primary mineral contents and contaminants. Size fractions with the largest proportion of glass shards were processed to recover glass shards and Fe–Ti oxide minerals. Samples with high amounts of organic material were soaked in 30% H_2O_2 overnight and then repeatedly rinsed with H_2O, resieved, and dried. A hand magnet was used to recover magnetite, while ilmenite and glass shards were recovered using a Frantz Isodynamic Magnetic Separator. Rock fragments contaminated the glass fraction in about a third of the samples. A solution of s-tetrabromoethane and acetone, mixed to approximately 2.4 g/ml, was used to remove the rock fragments. The glass fraction was washed repeatedly with acetone and then with H_2O to remove s-tetrabromoethane and acetone residues, respectively. Finally, the glass fraction was rinsed for 30 seconds with 1% trace-metal grade hydrofluoric acid (Fisher) to remove surface contaminants from the glass shards, rinsed repeatedly with H_2O, and air dried. All water was reverse osmosis (University of Toronto) or deionized (University of Alberta). Splits of the magnetite, ilmenite and glass fractions were mounted in epoxy blocks, polished and carbon coated for major-element analysis. A split of the glass fraction was hand picked under a stereoscopic microscope to remove any remaining contaminants prior to trace-element analysis.

3.2. Electron probe microanalysis

Glass shards from OCt samples collected at the Palisades site, Chester Bluff, and Caribou Creek 1 and 2 were analyzed at the University of Alberta on a JEOL 8900 superprobe by wavelength dispersive spectrometry (WDS). Glass shards from all other sites and all of the Fe–Ti oxide minerals were analysed at the University of Toronto by WDS using a Cameca SX50. Glass-shard analyses were performed with 15 keV accelerating voltage, 6 nA beam current and a 10 micron defocused beam. Standardization was achieved through mineral and glass standards. The rhyolitic obsidian, UA5831, was used to monitor the calibration in all analytical runs to evaluate any day to day differences in the calibration, and to evaluate any differences between the Alberta and Toronto data. The large number of samples precluded running all samples in a single analytical batch. All EPMA glass analyses are normalized to 100 wt. % anhydrous, with H_2O by difference (H_2O_d) being given, which is about 5 wt.% for many of the glass analyses. Fe-Ti oxide mineral

Table 2
Solution ICP-MS trace-element composition of purified glass shards from Old Crow tephra samples, ppm.

Site #	26	1	2	3	4	5	6	7	9	10	10	11	11
Site name	Type	Goodnews Bay	Togiak Bay	Hagemeister Island	Holitna	Imruk Lake	Baldwin Pen.	NK26B	Hogatza Mine	Ky-11	Ky-11	Palisades	Palisades
Sample	UT1	UT1407	UT1434	UT1577	UT613	UT371	UT976	UT1714	UT718	UT1834B	UT1834D	UA1124	UA1198
Sc	5.98	6.47	6.68	5.83	5.59	5.70	5.85	5.88	5.73	5.84	5.81	6.02	5.95
Rb	103	103	93	98	97	99	103	101	97	101	102	102	101
Sr	138	145	133	168	132	137	135	136	130	139	145	139	138
Y	34.7	36.0	30.8	34.8	33.6	34.6	35.4	34.8	32.9	35.7	35.6	35.1	34.6
Zr	259	259	231	243	244	249	254	251	240	259	256	252	250
Cs	4.37	4.13	4.30	4.13	4.25	4.16	4.42	4.29	4.24	4.28	4.20	4.34	4.34
Ba	923	1060	935	969	912	989	990	1015	966	903	899	989	978
La	24.7	26.1	24.7	24.9	24.8	24.9	25.2	25.3	24.7	24.8	24.9	25.2	25.0
Ce	52.8	55.2	53.2	54.0	53.2	52.3	52.9	52.9	52.2	53.3	54.7	53.8	53.5
Pr	5.83	6.11	5.78	6.09	5.91	5.94	5.91	5.96	5.86	5.89	5.95	6.00	5.99
Nd	23.7	25.1	23.5	24.9	23.7	24.1	24.2	24.3	24.0	24.2	24.5	24.4	24.5
Sm	5.57	5.84	5.63	6.27	5.74	5.95	6.08	5.72	5.73	5.78	5.89	5.79	5.96
Eu	0.87	1.03	0.88	1.01	0.90	0.94	1.01	1.00	0.96	0.87	0.89	0.94	0.94
Gd	4.83	5.58	4.72	5.36	4.85	4.92	4.98	5.18	5.12	4.82	4.92	5.13	5.05
Tb	0.90	0.99	0.86	0.94	0.91	0.89	0.96	0.96	0.89	0.92	0.92	0.96	0.93
Dy	5.34	6.00	5.18	5.58	5.43	5.53	5.34	5.54	5.39	5.48	5.53	5.55	5.49
Ho	1.27	1.41	1.23	1.31	1.28	1.37	1.33	1.32	1.27	1.29	1.31	1.34	1.35
Er	3.44	3.83	3.35	3.47	3.51	3.52	3.54	3.59	3.49	3.51	3.58	3.62	3.55
Tm	0.56	0.58	0.55	0.58	0.58	0.52	0.54	0.56	0.54	0.57	0.57	0.56	0.53
Yb	3.60	3.89	3.41	3.81	3.61	3.79	3.69	3.82	3.54	3.57	3.66	3.74	3.73
Lu	0.57	0.64	0.52	0.59	0.57	0.55	0.58	0.57	0.53	0.58	0.58	0.58	0.62
Hf	7.00	7.82	6.47	6.95	6.92	7.09	6.73	6.76	6.54	7.10	7.02	7.49	7.50
Th	9.81	10.56	8.66	10.17	9.88	10.77	9.23	9.66	8.97	10.22	10.22	9.88	11.03
U	4.28	4.59	3.99	4.37	4.34	4.93	4.21	3.95	3.89	4.40	4.44	4.42	4.68

Site #	12	13	13	13	13	13	15	19	20	21	22	22	22
Site name	Halfway House	Eva	Eva	Eva	Eva	Eva	Birch Ck.	Chester Bluff	Mile 293	Mirror Ck.	Thistle Creek	Thistle Creek	Thistle Creek
Sample	UT815	UT828	UT1727	UT1730	UT1731	UT1733	UT543	UA1099	UT524	UA339	UT1805	UT1816	UT1823
Sc	6.59	5.89	5.63	6.10	6.08	5.96	5.56	5.69	5.98	5.89	6.14	5.72	5.71
Rb	110	104	100	105	98	93	96	102	101	98	99	101	103
Sr	149	141	132	143	140	125	142	131	136	144	167	157	135
Y	37.1	35.8	34.3	35.6	34.8	32.2	35.9	34.8	34.9	34.9	35.5	35.7	35.2
Zr	270	264	247	259	247	235	253	256	252	239	243	248	255
Cs	4.58	4.48	4.17	4.18	4.31	4.23	4.47	4.28	4.28	4.20	4.08	4.30	4.42
Ba	1002	941	951	898	915	921	925	966	981	956	1038	1026	1002
La	27.4	25.4	24.2	24.3	25.3	25.1	25.8	24.7	25.3	25.4	25.5	26.1	25.3
Ce	59.8	54.7	51.4	53.0	53.7	53.7	54.1	51.5	54.3	54.8	52.9	54.7	53.8
Pr	6.46	6.09	5.79	5.76	5.95	5.94	6.09	5.78	6.08	6.11	6.10	6.11	6.01
Nd	26.7	24.7	23.4	23.8	24.4	24.2	24.7	23.1	24.9	25.2	25.1	25.6	24.6
Sm	6.49	5.84	5.68	5.64	5.72	5.77	5.74	5.72	5.90	6.18	6.04	5.83	5.90
Eu	1.02	0.90	0.96	0.89	0.88	0.87	0.90	0.96	0.95	0.96	1.03	1.03	1.00
Gd	5.41	4.85	4.85	4.81	4.85	4.89	4.74	5.07	5.43	5.35	5.18	5.43	5.39
Tb	1.02	0.92	0.89	0.90	0.90	0.89	0.92	0.91	0.94	0.95	0.91	0.96	0.97
Dy	6.13	5.62	5.34	5.41	5.47	5.38	5.55	5.43	5.57	5.67	5.63	5.67	5.57
Ho	1.42	1.30	1.27	1.27	1.28	1.29	1.31	1.26	1.36	1.34	1.32	1.35	1.37
Er	3.93	3.61	3.36	3.46	3.50	3.47	3.53	3.64	3.73	3.61	3.52	3.56	3.69
Tm	0.63	0.58	0.53	0.56	0.56	0.56	0.57	0.55	0.58	0.57	0.59	0.53	0.57
Yb	3.96	3.68	3.46	3.65	3.60	3.49	3.56	3.51	3.76	3.70	3.44	3.80	3.75
Lu	0.64	0.58	0.54	0.57	0.56	0.55	0.57	0.60	0.61	0.56	0.55	0.58	0.61
Hf	7.55	7.28	6.47	6.91	6.78	6.64	7.01	7.32	7.12	6.83	7.08	7.15	7.50
Th	10.59	10.26	8.52	9.11	9.31	9.12	10.27	9.79	10.96	9.46	9.82	10.27	10.91
U	4.62	4.48	3.88	4.07	4.06	4.19	4.52	4.38	4.88	4.28	4.17	4.49	4.68

(*continued on next page*)

Table 2 (*continued*)

Site #	23	24	25	QLO-1	QLO-1	QLO-1		RGM-1	RGM-1	RGM-1				
Site name	Caribou Ck. 1	Caribou Ck. 2	Klondike	OCt 2008	March 2008	USGS Recc	+/-	OCt 2008	March 2008	USGS Recc	+/-	Precision from QLO1 and RGM1*	Average OCt	+/-
Sample	UA1240B	UA1274	UT17											
Sc	6.14	6.15	6.09	8.76	8.30	8.9		4.90	4.45	4.4	0.3	5.30%	5.95	0.32
Rb	99	99	105	73.0	72.3	74	3	153	154	150	8	0.37%	100.49	0.37
Sr	140	147	144	344	331	340	12	106	111	110	10	2.94%	140.92	4.14
Y	35.1	34.5	34.1	23.0	24.0	24	3	23.1	23.4	*25*		2.02%	34.78	0.70
Zr	252	247	252	174	184	185	16	227	225	220	20	2.25%	250.50	5.63
Cs	4.14	4.23	4.21	1.71	1.60	1.8	0.2	10.4	9.9	9.6	0.6	3.98%	4.28	0.17
Ba	991	1024	1043	1386	1345	1370	80	871	850	810	46	1.95%	969.22	18.88
La	24.9	24.9	24.5	27.3	26.3	27	2	25.7	23.1	24	1.1	4.95%	25.14	1.25
Ce	51.9	53.3	53.1	52.8	51.0	54	6	51.5	47.2	47	4	4.27%	53.60	2.29
Pr	5.83	5.94	5.78	5.62	5.48	6.01	0.11	5.25	4.86	4.7		3.58%	5.97	0.21
Nd	24.1	24.3	23.5	22.6	22.0	26		20.0	18.5	19	1	3.81%	24.39	0.93
Sm	5.85	6.01	5.58	4.87	4.83	4.9	0.2	4.51	4.20	4.3	0.3	2.79%	5.86	0.16
Eu	1.01	0.95	0.93	1.36	1.31	1.43	0.12	0.70	0.72	0.66	0.08	2.67%	0.95	0.03
Gd	5.33	5.08	4.77	4.41	4.38	4.7		3.82	3.77	3.7	0.4	0.76%	5.07	0.04
Tb	0.92	0.91	0.89	0.72	0.66	0.71	0.07	0.66	0.64	0.66		3.82%	0.93	0.04
Dy	5.48	5.50	5.38	4.00	3.83	3.8	0.3	3.87	3.76	4.1	0.1	2.46%	5.52	0.14
Ho	1.27	1.31	1.26	0.91	0.87	0.86	0.22	0.87	0.86	0.95		2.08%	1.31	0.03
Er	3.56	3.47	3.47	2.42	2.36	2.3	0.1	2.48	2.42	2.6		1.61%	3.56	0.06
Tm	0.57	0.53	0.56	0.38	0.35	0.4		0.39	0.38	0.37		4.28%	0.56	0.02
Yb	3.33	3.70	3.57	2.36	2.35	2.3	0.2	2.52	2.57	2.6	0.3	0.85%	3.65	0.03
Lu	0.55	0.57	0.57	0.37	0.35	0.37	0.04	0.39	0.40	0.4	0.03	3.21%	0.58	0.02
Hf	6.95	6.99	6.81	4.47	4.40	4.6		6.31	6.15	6.2		1.46%	7.03	0.10
Th	8.82	10.15	9.21	4.12	4.59	4.5	0.5	13.8	15.9	15	1.3	8.83%	9.85	0.87
U	4.52	4.52	4.14	1.75	1.88	1.9	0.12	5.75	6.61	5.8	0.5	7.55%	4.36	0.33

Notes: * Analytical precision (as coefficient of variation) calculated from repeat analyses of QLO-1 and RGM-1.
This represents the intermediate precision which can be expected from repeat preparations and analyses of the same homogeneous material at different times.
Note the similarity in the RSD for all Old Crow samples and the precision based on analyses of QLO-1 and RGM-1.

Table 3
Major-element composition of glass shards in Old Crow tephra samples, wt. %.

Site #	26	1	2	3	4	5	6	7
Site name	Type locality	Goodnews Bay	Togiak Bay	Hagemeister Is.	Holitna	Imruk Lake	Baldwin Pen.	NK26B
SiO_2	75.37 (0.22)	75.44 (0.25)	75.36 (0.23)	75.53 (0.22)	75.46 (0.21)	75.33 (0.24)	75.36 (0.23)	75.41 (0.21)
TiO_2	0.33 (0.09)	0.30 (0.09)	0.33 (0.07)	0.32 (0.09)	0.27 (0.09)	0.27 (0.11)	0.28 (0.10)	0.33 (0.08)
Al_2O_3	13.03 (0.11)	13.07 (0.14)	13.09 (0.12)	13.07 (0.13)	13.06 (0.15)	13.17 (0.11)	13.15 (0.17)	13.08 (0.12)
FeOt	1.71 (0.08)	1.74 (0.04)	1.75 (0.08)	1.72 (0.07)	1.75 (0.06)	1.73 (0.07)	1.70 (0.08)	1.70 (0.06)
MnO	0.05 (0.04)	0.07 (0.04)	0.06 (0.04)	0.06 (0.04)	0.06 (0.04)	0.06 (0.05)	0.05 (0.04)	0.06 (0.04)
CaO	1.50 (0.08)	1.47 (0.03)	1.47 (0.06)	1.44 (0.06)	1.48 (0.05)	1.45 (0.05)	1.46 (0.05)	1.48 (0.05)
MgO	0.29 (0.02)	0.26 (0.02)	0.27 (0.03)	0.28 (0.02)	0.29 (0.03)	0.27 (0.03)	0.29 (0.03)	0.28 (0.03)
Na_2O	3.68 (0.13)	3.75 (0.18)	3.73 (0.18)	3.65 (0.13)	3.66 (0.10)	3.74 (0.11)	3.74 (0.10)	3.66 (0.11)
K_2O	3.75 (0.09)	3.63 (0.11)	3.68 (0.09)	3.66 (0.10)	3.70 (0.10)	3.68 (0.12)	3.70 (0.14)	3.72 (0.13)
Cl	0.30 (0.04)	0.28 (0.04)	0.26 (0.04)	0.27 (0.03)	0.27 (0.03)	0.29 (0.04)	0.28 (0.04)	0.28 (0.04)
H_2Od	4.60 (1.26)	3.55 (1.04)	4.51 (1.29)	4.69 (0.84)	5.25 (1.26)	5.72 (0.86)	5.04 (1.00)	4.07 (1.59)
n	39	10	38	16	18	17	15	16
Site #	8	9	10	11	12	13	14	15
Site name	NK29A	Hogatza Mine	Ky-11	Palisades	Halfway House	Eva	West Dawson	Birch Hill
SiO_2	75.44 (0.16)	75.40 (0.22)	75.47 (0.20)	75.19 (0.21)	75.50 (0.22)	75.49 (0.23)	75.56 (0.20)	75.59 (0.24)
TiO_2	0.31 (0.07)	0.31 (0.10)	0.31 (0.07)	0.30 (0.05)	0.31 (0.09)	0.30 (0.08)	0.27 (0.07)	0.28 (0.06)
Al_2O_3	13.00 (0.13)	13.10 (0.11)	13.03 (0.13)	13.10 (0.11)	13.00 (0.14)	13.03 (0.12)	13.06 (0.13)	13.04 (0.10)
FeOt	1.71 (0.06)	1.72 (0.07)	1.72 (0.07)	1.76 (0.06)	1.68 (0.07)	1.71 (0.07)	1.73 (0.11)	1.71 (0.07)
MnO	0.05 (0.03)	0.04 (0.03)	0.06 (0.04)	0.06 (0.03)	0.06 (0.04)	0.06 (0.04)	0.05 (0.03)	0.06 (0.05)
CaO	1.48 (0.08)	1.45 (0.08)	1.50 (0.06)	1.50 (0.05)	1.47 (0.07)	1.47 (0.08)	1.47 (0.07)	1.48 (0.05)
MgO	0.29 (0.03)	0.28 (0.04)	0.28 (0.02)	0.29 (0.02)	0.29 (0.03)	0.29 (0.03)	0.28 (0.03)	0.29 (0.03)
Na_2O	3.73 (0.11)	3.75 (0.11)	3.63 (0.13)	3.82 (0.10)	3.76 (0.16)	3.71 (0.14)	3.67 (0.10)	3.60 (0.11)
K_2O	3.72 (0.08)	3.64 (0.09)	3.73 (0.09)	3.69 (0.10)	3.65 (0.11)	3.66 (0.11)	3.75 (0.09)	3.69 (0.12)
Cl	0.29 (0.03)	0.30 (0.04)	0.28 (0.04)	0.29 (0.03)	0.28 (0.04)	0.28 (0.04)	0.28 (0.04)	0.28 (0.05)
H_2Od	4.59 (0.91)	5.25 (1.06)	5.77 (0.88)	4.23 (1.44)	4.12 (1.23)	4.28 (1.19)	5.11 (0.57)	3.49 (1.14)
n	16	18	86	36	141	107	9	12
Site #	16	17	18	19	20	21	22	22
Site name	Sheep Ck. Valley	Gold Hill	Birch Creek	Chester Bluff	Mile 293	Mirror Creek	Thistle (UT1805)	Thistle (UT1816)
SiO_2	75.62 (0.20)	75.55 (0.16)	75.48 (0.25)	75.23 (0.32)	75.34 (0.17)	75.33 (0.19)	75.48 (0.25)	75.48 (0.19)
TiO_2	0.30 (0.10)	0.28 (0.07)	0.28 (0.07)	0.30 (0.05)	0.31 (0.10)	0.26 (0.10)	0.30 (0.11)	0.29 (0.08)
Al_2O_3	13.00 (0.13)	12.99 (0.08)	13.09 (0.09)	13.08 (0.19)	13.22 (0.18)	13.16 (0.13)	13.01 (0.08)	13.03 (0.14)
FeOt	1.67 (0.06)	1.68 (0.06)	1.69 (0.10)	1.77 (0.09)	1.71 (0.06)	1.72 (0.07)	1.74 (0.08)	1.69 (0.07)
MnO	0.07 (0.05)	0.04 (0.04)	0.07 (0.04)	0.06 (0.03)	0.07 (0.05)	0.05 (0.03)	0.07 (0.05)	0.06 (0.06)
CaO	1.44 (0.08)	1.49 (0.06)	1.46 (0.06)	1.54 (0.07)	1.44 (0.06)	1.44 (0.05)	1.55 (0.11)	1.46 (0.05)
MgO	0.30 (0.02)	0.28 (0.03)	0.30 (0.02)	0.28 (0.03)	0.28 (0.02)	0.29 (0.03)	0.29 (0.02)	0.30 (0.03)
Na_2O	3.69 (0.14)	3.78 (0.08)	3.64 (0.13)	3.75 (0.16)	3.71 (0.11)	3.80 (0.09)	3.62 (0.16)	3.67 (0.11)
K_2O	3.63 (0.13)	3.63 (0.09)	3.76 (0.17)	3.70 (0.11)	3.64 (0.06)	3.69 (0.10)	3.66 (0.09)	3.73 (0.09)
Cl	0.28 (0.04)	0.27 (0.03)	0.25 (0.03)	0.28 (0.03)	0.27 (0.04)	0.26 (0.04)	0.29 (0.03)	0.28 (0.03)
H_2Od	4.58 (0.89)	3.05 (1.25)	5.22 (1.88)	4.59 (1.49)	4.94 (1.36)	5.04 (1.00)	5.10 (1.76)	4.08 (1.26)
n	15	15	18	88	16	14	14	18
Site #	22	23	24	25	27			
Site name	Thistle (UT1823)	Caribou Ck. 1	Caribou Ck.2	Klondike	Old Crow Basin	All Samples		
SiO_2	75.25 (0.27)	75.29 (0.25)	75.47 (0.26)	75.28 (0.21)	75.66 (0.18)	75.42 (0.26)		
TiO_2	0.30 (0.10)	0.29 (0.05)	0.29 (0.04)	0.27 (0.09)	0.27 (0.06)	0.30 (0.08)		
Al_2O_3	13.07 (0.13)	13.03 (0.11)	12.94 (0.16)	13.04 (0.08)	13.00 (0.13)	13.05 (0.14)		
FeOt	1.71 (0.06)	1.75 (0.09)	1.73 (0.06)	1.79 (0.06)	1.67 (0.06)	1.72 (0.08)		
MnO	0.05 (0.04)	0.07 (0.04)	0.07 (0.04)	0.04 (0.04)	0.05 (0.05)	0.06 (0.04)		
CaO	1.51 (0.06)	1.55 (0.08)	1.52 (0.06)	1.50 (0.08)	1.51 (0.06)	1.49 (0.07)		
MgO	0.28 (0.03)	0.29 (0.03)	0.29 (0.03)	0.27 (0.03)	0.28 (0.03)	0.29 (0.03)		
Na_2O	3.82 (0.10)	3.74 (0.23)	3.69 (0.14)	3.78 (0.05)	3.61 (0.09)	3.72 (0.15)		
K_2O	3.73 (0.12)	3.72 (0.10)	3.72 (0.13)	3.74 (0.07)	3.67 (0.13)	3.69 (0.11)		
Cl	0.29 (0.03)	0.27 (0.03)	0.27 (0.03)	0.28 (0.04)	0.27 (0.03)	0.28 (0.04)		
H_2Od	4.45 (1.69)	4.91 (1.40)	4.72 (0.97)	4.16 (0.57)	4.57 (0.62)	4.61 (1.34)		
n	26	35	46	10	15	924		

Notes: Analyses for sites # 11, 19, 25 and 26 performed using a JEOL 8900 with all other analyses performed using a Cameca SX-50. Standard deviation is number in brackets. FeOt, total Fe as FeO; n, number of analyses. Average composition based on the following samples: Type locality (UT1),Goodnews Bay (UT1407); Togiak Bay (UT1434), Hagemeister Island (UT1577); Holitna (UT613); Imruk Lake (UT371); Baldwin Pen. (UT976), NK26B (UT1714); NK29A (UT1718); Hogatza Mine (UT718); Ky-11 (UT1833, UT1834a, UT1834b, UT1834c, UT1834d); Palisades (UA1124, UA1198); Halfway House (UT815, UT896, UT897, UT898, UT899, UT900, UT901); Eva (UT388, UT410, UT828, UT1727, UT1730, UT1731, UT1733);West Dawson (UT420); Birch Hill (UT1002); Sheep Ck. Valley (UA368); Gold Hill (UA348); Birch Creek (UT543); Chester Bluff (UA1099, UA1233, UA1211); Mile 293 Richardson Hwy. (UT524); Mirror Creek (UA339); Caribou Ck. 1 (UA1240); Caribou Ck. 2 (UA1274); Klondike (UT17); Old Crow Basin (UT50).

analyses were obtained using a 15 keV accelerating voltage, 25 nA beam current and a 1 micron beam. Standardization was achieved through synthetic oxides and mineral standards. Several standards were included in each analytical run to monitor the calibration. In some samples, a large proportion of the Fe–Ti oxide grains appeared to be contaminants. Primary Fe–Ti oxide crystals have glass selvages attached to them, while contaminant grains do not have selvages or are attached to minerals. The Cameca SX50 can switch between WDS and energy dispersive spectrometry (EDS) during the course of an analytical run. Hence, selvages were analyzed by EDS prior to WDS analysis of the Fe-Ti oxide.

3.3. ICP-MS method

Trace-element analyses presented here are from analysis of digested separates of glass by solution nebulisation ICP-MS.

Table 4
Major-element composition of titano-magnetite in samples of Old Crow tephra, wt. %.

Site #	26	2	3	4	5	6	7	8
Site name	Type locality	Togiak Bay	Hagemeister Is.	Holitna	Imruk Lake	Baldwin Pen.	NK26B	NK29A
SiO_2	0.18 (0.10)	0.12 (0.05)	0.09 (0.03)	0.14 (0.04)	0.11 (0.03)	0.11 (0.02)	0.11 (0.01)	0.11 (0.02)
TiO_2	9.23 (0.18)	9.43 (0.07)	9.49 (0.23)	9.37 (0.16)	9.29 (0.23)	9.50 (0.26)	9.07 (0.22)	9.24 (0.22)
Al_2O_3	2.14 (0.51)	1.97 (0.03)	1.90 (0.16)	2.01 (0.03)	2.01 (0.05)	2.01 (0.03)	2.00 (0.04)	1.96 (0.07)
Cr_2O_3	0.03 (0.03)	0.03 (0.03)	0.07 (0.03)	0.02 (0.02)	0.07 (0.02)	0.07 (0.03)	0.06 (0.03)	0.03 (0.04)
V_2O_3	0.40 (0.17)	0.34 (0.03)	0.38 (0.05)	0.34 (0.04)	0.38 (0.02)	0.35 (0.05)	0.36 (0.04)	0.32 (0.07)
Fe_2O_3	47.88 (0.92)	48.33 (0.40)	48.79 (0.36)	48.35 (0.24)	48.35 (0.40)	48.05 (0.85)	48.73 (0.50)	48.64 (0.31)
FeO	36.68 (0.33)	37.12 (0.20)	37.46 (0.50)	37.08 (0.21)	36.94 (0.41)	37.17 (0.23)	36.46 (0.58)	36.79 (0.44)
MgO	1.61 (0.16)	1.52 (0.05)	1.44 (0.14)	1.54 (0.05)	1.52 (0.04)	1.52 (0.03)	1.66 (0.19)	1.53 (0.04)
MnO	0.60 (0.06)	0.62 (0.02)	0.67 (0.10)	0.60 (0.04)	0.62 (0.02)	0.61 (0.05)	0.62 (0.08)	0.69 (0.11)
CaO	0.07 (0.04)	0.03 (0.02)	0.01 (0.01)	0.03 (0.02)	0.03 (0.02)	0.03 (0.01)	0.01 (0.01)	0.03 (0.02)
NiO	0.01 (0.02)	0.04 (0.05)	0.05 (0.02)	0.03 (0.03)	0.01 (0.01)	0.02 (0.02)	0.01 (0.02)	0.02 (0.03)
total	98.82 (0.50)	99.56 (0.53)	100.36 (0.84)	99.51 (0.36)	99.32 (0.60)	99.43 (0.60)	99.09 (0.64)	99.37 (0.87)
FeOt	79.76 (0.95)	80.61 (0.44)	81.36 (0.73)	80.58 (0.28)	80.45 (0.55)	80.41 (0.75)	80.31 (0.39)	80.56 (0.62)
n	12	11	3	11	6	7	5	7
Site #	9	10	11	11	12	13	18	19
Site name	Hogatza Mine	Ky-11	Palisades	Palisades	Halfway House	Eva	Birch Creek	Chester Bluff
SiO_2	0.10 (0.02)	0.13 (0.03)	0.12	0.09 (0.02)	0.09 (0.02)	0.11 (0.05)	0.11 (0.02)	0.10 (0.02)
TiO_2	9.42 (0.10)	9.35 (0.34)	11.00	9.47 (0.16)	9.54 (0.11)	9.30 (0.17)	9.30 (0.15)	9.30 (0.11)
Al_2O_3	1.94 (0.15)	2.00 (0.12)	2.21	2.01 (0.04)	2.01 (0.03)	2.00 (0.04)	1.96 (0.02)	2.04 (0.06)
Cr_2O_3	0.07 (0.03)	0.02 (0.02)	0.07	0.07 (0.02)	0.06 (0.02)	0.03 (0.03)	0.02 (0.02)	0.05 (0.02)
V_2O_3	0.38 (0.06)	0.33 (0.07)	0.21	0.35 (0.04)	0.37 (0.04)	0.35 (0.04)	0.34 (0.03)	0.34 (0.08)
Fe_2O_3	48.82 (0.19)	48.47 (0.82)	45.38	48.50 (0.32)	48.33 (0.55)	48.56 (0.38)	48.58 (0.45)	48.86 (0.28)
FeO	37.21 (0.27)	37.01 (0.34)	38.25	37.26 (0.27)	37.25 (0.38)	36.94 (0.31)	36.92 (0.36)	37.04 (0.22)
MgO	1.58 (0.06)	1.57 (0.08)	1.63	1.54 (0.05)	1.53 (0.03)	1.56 (0.05)	1.56 (0.04)	1.56 (0.10)
MnO	0.62 (0.04)	0.63 (0.06)	0.97	0.59 (0.04)	0.61 (0.03)	0.62 (0.05)	0.62 (0.06)	0.63 (0.04)
CaO	0.02 (0.02)	0.02 (0.03)	0.02	0.03 (0.02)	0.06 (0.03)	0.03 (0.05)	0.02 (0.01)	0.03 (0.01)
NiO	0.04 (0.04)	0.02 (0.03)	0.00	0.03 (0.03)	0.02 (0.02)	0.02 (0.02)	0.02 (0.02)	0.03 (0.02)
total	100.19 (0.54)	99.54 (0.52)	99.85	99.95 (0.41)	99.87 (0.87)	99.52 (0.57)	99.46 (0.70)	99.96 (0.43)
FeOt	81.14 (0.43)	80.62 (0.68)	79.09	80.90 (0.34)	80.74 (0.85)	80.64 (0.49)	80.64 (0.62)	81.00 (0.35)
n	7	29	1	7	7	82	13	7
Site #	20	21	22	22	22	24	25	
Site name	Mile 293	Mirror Creek	Thistle (UT1805)	Thistle (UT1816)	Thistle (UT1823)	Caribou Ck. 2	Klondike	
SiO_2	0.09 (0.01)	0.10 (0.02)	0.09 (0.02)	0.10 (0.01)	0.10 (0.01)	0.10 (0.02)	0.11 (0.02)	
TiO_2	9.42 (0.12)	9.32 (0.06)	9.47 (0.06)	9.53 (0.12)	9.14 (0.36)	9.36 (0.18)	9.29 (0.18)	
Al_2O_3	1.99 (0.02)	2.01 (0.05)	1.98 (0.03)	1.98 (0.02)	1.99 (0.05)	2.01 (0.07)	2.00 (0.05)	
Cr_2O_3	0.05 (0.03)	0.06 (0.03)	0.09 (0.03)	0.07 (0.03)	0.07 (0.03)	0.08 (0.04)	0.06 (0.02)	
V_2O_3	0.38 (0.04)	0.33 (0.07)	0.38 (0.04)	0.36 (0.04)	0.35 (0.02)	0.35 (0.04)	0.36 (0.04)	
Fe_2O_3	48.64 (0.20)	48.24 (0.34)	48.39 (0.24)	48.05 (0.35)	48.59 (0.32)	47.93 (0.53)	48.58 (0.33)	
FeO	37.14 (0.27)	36.88 (0.06)	37.15 (0.17)	37.17 (0.23)	36.73 (0.49)	36.81 (0.20)	36.86 (0.30)	
MgO	1.55 (0.03)	1.54 (0.03)	1.55 (0.05)	1.54 (0.03)	1.53 (0.07)	1.55 (0.05)	1.59 (0.05)	
MnO	0.64 (0.08)	0.60 (0.04)	0.62 (0.04)	0.60 (0.03)	0.60 (0.02)	0.59 (0.04)	0.62 (0.03)	
CaO	0.02 (0.02)	0.03 (0.02)	0.04 (0.01)	0.02 (0.02)	0.02 (0.02)	0.04 (0.02)	0.04 (0.01)	
NiO	0.04 (0.03)	0.03 (0.02)	0.02 (0.03)	0.01 (0.02)	0.01 (0.02)	0.02 (0.03)	0.02 (0.03)	
Total	99.98 (0.46)	99.15 (0.31)	99.77 (0.30)	99.44 (0.47)	99.13 (0.73)	98.85 (0.46)	99.53 (0.48)	
FeOt	80.91 (0.33)	80.29 (0.35)	80.69 (0.31)	80.40 (0.40)	80.45 (0.39)	79.94 (0.50)	80.57 (0.43)	
n	7	7	6	6	5	7	8	

Notes: Total Fe split into FeO and Fe_2O_3 using the method of Carmichael (1967). Standard deviation is number in brackets. FeOt, total Fe as FeO; n, number of analyses. Average composition based on the following samples: Type locality (UT1),Togiak Bay (UT1434), Hagemeister Island (UT1577); Holitna (UT613); Imruk Lake (UT371); Baldwin Pen. (UT976), NK26B (UT1714); NK29A (UT1718); Hogatza Mine (UT718); Ky-11 (UT1833, UT1834b, UT1834d); Palisades (UA1124); Halfway House (UT815); Eva (UT828, UT1727, UT1730, UT1731, UT1733); Birch Creek (UT543); Chester Bluff (UA1099); Mile 293 Richardson Hwy. (UT524); Mirror Creek (UA339); Caribou Ck. 2 (UA1274); Klondike (UT17).

Solutions of glass separates were prepared by a hot open $HF/HClO_4$ digestion. If available, 0.2 g of sample was weighed into a PTFE beaker, to which 2 ml of HCl were added (to dissolve any oxide phases) and this was left to stand cold overnight before evaporation to dryness. When cool, 15 ml HF and 4 ml $HClO_4$ were added to the beaker, again left cold overnight, and then heated to evaporate to dryness. If necessary, a second batch of $HF/HClO_4$ was used to digest the sample completely. Two ml of $HClO_4$ were then added and evaporated to remove any residual F^- present, and the dry, soluble residue was taken into solution in 5% HNO_3, made up to volume, and stored for analysis. Final solution volumes were 50 ml for samples weighing about 0.1 g and 100 ml for sample weights of about 0.2 g, to give ~0.2% w/v dissolved solids for analysis. At this stage solutions were spiked with 100 ug/L of Ru to act as an internal standard, giving a solution ready for ICP-MS analysis. This preparation removes the need for any further dilution of the stock solution for analysis. All reagents used were Fisher Certified analytical reagents or Primar grade chemicals, all water was >18 Mohm cm^{-1}, and at least 2 blanks were prepared for each batch of samples.

Solution ICP-MS analyses were performed on a VG PlasmaQuad PQII+ STE at Aberystwyth University. Calibration curves were generated from 0 ug/L, 100 ug/L and 200 ug/L synthetic multi-element calibration standards. Two 45 second acquisitions were collected from each sample solution where 26 elements were determined in peak jumping mode, i.e., run in a mode where the spectrometer was set to jump from analyte peak to peak, giving the best sensitivity. Samples for solution ICP-MS analysis were prepared and analyzed in two batches (using identical methods) in March and October 2008. In each batch the USGS reference materials QLO-1 (quartz latite) and RGM-1 (rhyolite) were prepared and analysed. The trace-element concentrations determined from these reference

Table 5
Major-element composition of ilmenite in samples of Old Crow tephra, wt. %.

Site #	26	2	3	4	5	6	8	9
Site name	Type locality	Togiak Bay	Hagemeister Is.	Holitna	Imruk Lake	Baldwin Pen.	NK29A	Hogatza Mine
SiO_2	0.06 (0.02)	0.04 (0.03)	0.02 (0.02)	0.04 (0.05)	0.04 (0.02)	0.02 (0.02)	0.03 (0.01)	0.06 (0.04)
TiO_2	42.47 (0.45)	42.59 (0.23)	43.12 (0.61)	43.21 (0.05)	42.87 (0.20)	42.85 (0.27)	42.88 (0.51)	42.60 (0.27)
Al_2O_3	0.24 (0.01)	0.22 (0.02)	0.22 (0.02)	0.23 (0.00)	0.23 (0.02)	0.22 (0.03)	0.22 (0.01)	0.22 (0.02)
Cr_2O_3	0.02 (0.02)	0.01 (0.02)	0.04 (0.03)	0.02 (0.00)	0.04 (0.03)	0.03 (0.03)	0.03 (0.03)	0.02 (0.03)
V_2O_3	0.32 (0.01)	0.19 (0.08)	0.29 (0.03)	0.25 (0.06)	0.27 (0.04)	0.30 (0.04)	0.24 (0.07)	0.25 (0.03)
Fe_2O_3	20.59 (0.14)	19.62 (0.61)	19.56 (0.83)	19.41 (0.25)	20.13 (0.24)	19.86 (0.62)	19.67 (0.51)	19.89 (0.52)
FeO	33.05 (0.36)	33.09 (0.21)	33.47 (0.44)	33.53 (0.04)	33.30 (0.26)	33.15 (0.20)	33.23 (0.40)	33.01 (0.25)
MgO	2.44 (0.02)	2.50 (0.09)	2.53 (0.06)	2.55 (0.01)	2.49 (0.06)	2.57 (0.11)	2.56 (0.08)	2.55 (0.07)
MnO	0.74 (0.05)	0.74 (0.05)	0.76 (0.05)	0.78 (0.03)	0.75 (0.04)	0.74 (0.05)	0.73 (0.05)	0.74 (0.05)
CaO	0.06 (0.01)	0.02 (0.01)	0.02 (0.01)	0.02 (0.02)	0.05 (0.05)	0.06 (0.04)	0.04 (0.03)	0.03 (0.02)
NiO	0.05 (0.00)	0.02 (0.02)	0.02 (0.02)	0.04 (0.00)	0.02 (0.02)	0.00 (0.00)	0.02 (0.02)	0.03 (0.04)
total	100.03 (0.96)	99.05 (0.35)	100.06 (0.68)	100.07 (0.21)	100.19 (0.39)	99.79 (0.37)	99.63 (0.90)	99.40 (0.67)
FeOt	51.57 (0.49)	50.75 (0.51)	51.08 (0.52)	51.00 (0.19)	51.42 (0.30)	51.02 (0.43)	50.93 (0.42)	50.91 (0.55)
n	2	10	10	2	7	5	13	7
Site #	10	11	12	13	18	19	20	21
Site name	Ky-11	Palisades	Halfway House	Eva	Birch Creek	Chester Bluff	Mile 293	Mirror Creek
SiO_2	0.15 (0.20)	0.02 (0.02)	0.04 (0.02)	0.05 (0.02)	0.05 (0.02)	0.04 (0.02)	0.03 (0.02)	0.03 (0.02)
TiO_2	42.45 (0.51)	43.32 (0.35)	43.07 (0.36)	42.54 (0.62)	42.63 (0.39)	43.10 (0.22)	42.94 (0.35)	42.64 (0.48)
Al_2O_3	0.22 (0.02)	0.23 (0.02)	0.24 (0.02)	0.22 (0.02)	0.21 (0.02)	0.22 (0.01)	0.23 (0.02)	0.23 (0.02)
Cr_2O_3	0.02 (0.01)	0.04 (0.03)	0.04 (0.03)	0.02 (0.03)	0.01 (0.02)	0.05 (0.02)	0.04 (0.03)	0.04 (0.02)
V_2O_3	0.12 (0.02)	0.26 (0.02)	0.28 (0.03)	0.16 (0.07)	0.15 (0.06)	0.30 (0.03)	0.30 (0.04)	0.30 (0.02)
Fe_2O_3	19.45 (0.53)	19.18 (0.32)	19.64 (0.56)	19.74 (1.08)	19.76 (0.74)	19.67 (0.34)	19.84 (0.26)	19.75 (0.70)
FeO	32.96 (0.23)	33.67 (0.28)	33.53 (0.32)	33.00 (0.43)	33.10 (0.25)	33.55 (0.26)	33.25 (0.33)	33.05 (0.27)
MgO	2.59 (0.06)	2.53 (0.07)	2.48 (0.04)	2.51 (0.09)	2.51 (0.05)	2.49 (0.04)	2.57 (0.04)	2.54 (0.13)
MnO	0.71 (0.05)	0.72 (0.03)	0.74 (0.04)	0.76 (0.11)	0.74 (0.04)	0.74 (0.03)	0.76 (0.02)	0.75 (0.04)
CaO	0.03 (0.01)	0.04 (0.02)	0.05 (0.04)	0.04 (0.04)	0.05 (0.03)	0.04 (0.02)	0.03 (0.01)	0.03 (0.02)
NiO	0.01 (0.02)	0.02 (0.03)	0.02 (0.02)	0.02 (0.03)	0.01 (0.02)	0.02 (0.03)	0.02 (0.03)	0.01 (0.01)
total	98.72 (0.56)	100.04 (0.69)	100.12 (0.31)	99.05 (0.42)	99.21 (0.34)	100.23 (0.27)	100.01 (0.57)	99.35 (0.50)
FeOt	50.46 (0.52)	50.93 (0.39)	51.20 (0.30)	50.76 (0.72)	50.88 (0.50)	51.26 (0.25)	51.11 (0.25)	50.82 (0.55)
n	4	7	6	26	10	8	7	6
Site #	22	22	22	24	25			
Site name	Thistle (UT1805)	Thistle (UT1816)	Thistle (UT1823)	Caribou Ck. 2	Klondike			
SiO_2	0.02 (0.02)	0.03 (0.02)	0.04 (0.03)	0.04 (0.02)	0.02 (0.02)			
TiO_2	42.87 (0.25)	42.99 (0.49)	42.69 (0.61)	43.06 (0.26)	42.49 (0.31)			
Al_2O_3	0.22 (0.01)	0.23 (0.02)	0.22 (0.03)	0.23 (0.01)	0.21 (0.02)			
Cr_2O_3	0.04 (0.03)	0.05 (0.03)	0.04 (0.03)	0.04 (0.02)	0.03 (0.03)			
V_2O_3	0.27 (0.03)	0.28 (0.03)	0.26 (0.03)	0.26 (0.03)	0.29 (0.01)			
Fe_2O_3	19.85 (0.53)	19.41 (0.45)	19.52 (0.49)	19.44 (0.33)	19.97 (0.35)			
FeO	33.31 (0.24)	33.35 (0.44)	33.07 (0.53)	33.55 (0.27)	32.95 (0.31)			
MgO	2.49 (0.01)	2.53 (0.05)	2.54 (0.04)	2.48 (0.09)	2.51 (0.04)			
MnO	0.75 (0.04)	0.78 (0.03)	0.76 (0.01)	0.75 (0.05)	0.73 (0.04)			
CaO	0.03 (0.02)	0.04 (0.03)	0.04 (0.04)	0.03 (0.01)	0.04 (0.01)			
NiO	0.03 (0.03)	0.01 (0.02)	0.01 (0.02)	0.01 (0.01)	0.02 (0.01)			
Total	99.86 (0.23)	99.68 (0.67)	99.19 (0.92)	99.88 (0.54)	99.27 (0.73)			
FeOt	51.17 (0.30)	50.81 (0.34)	50.63 (0.42)	51.04 (0.31)	50.93 (0.45)			
n	7	7	5	5	4			

Notes: Total Fe split into FeO and Fe2O3 using the method of Carmichael (1967). Standard deviation is number in brackets. FeOt, total Fe as FeO; n, number of analyses. Average composition based on the following samples: Type locality (UT1),Togiak Bay (UT1434), Hagemeister Island (UT1577); Holitna (UT613); Imruk Lake (UT371); Baldwin Pen. (UT976); NK29A (UT1718); Hogatza Mine (UT718); Ky-11 (UT1834b, UT1834d); Palisades (UA1124); Halfway House (UT815); Eva (UT828, UT1727, UT1730, UT1731, UT1733); Birch Creek (UT543); Chester Bluff (UA1099); Mile 293 Richardson Hwy. (UT524); Mirror Creek (UA339); Caribou Ck. 2 (UA1274); Klondike (UT17).

materials are listed in Table 2, and this gives an indication of the analytical accuracy of the ICP-MS method used here, which is typically between ±2 to 5%. This is generally within the errors given for the recommended concentrations for these reference materials (see Table 2 and http://minerals.cr.usgs.gov/geo_chem_stand). Analytical precision based on repeated analyses of these reference materials is also given in Table 2 and is in the ±1–5% range, which is an indication of the precision that can be expected for an individual analysis. Further details of analytical methods are given in Pearce et al. (2004).

4. Results

4.1. Old Crow tephra samples

New compositional data on glass, magnetite, and ilmenite from all but one of the published OCt occurrences, including site 8 on the Noatak River, Alaska (Fig. 1; Table 1), are given in Tables 2–5. The exception is the Moose Creek site of Begét and Keskinen (2003). Individual analyses of OCt glass shards, magnetite and ilmenite crystals are given in Supplementary Tables 1–3, respectively. Earlier identification of samples UA338 from the southern Yukon, and UT361 from the Ogilvie River, Yukon, as OCt proved to be incorrect (Westgate et al., 1985). UA338 has no known correlatives and UT361 is Dawson tephra (Westgate et al., 2000).

Old Crow tephra glass shards have a rhyolitic composition and major-element bivariate plots show a limited compositional range, correlative samples being uniformly distributed around UT1, a sample from the type locality (Fig. 2, Table 3). Concentrations of the major elements in glass shards of most samples average within 1 σ of the average composition of UT1 (Table 3), but a few samples show a slightly greater compositional difference (e.g. Goodnews Bay, Hogatza Mine, and Palisades). Trace-element contents of glass

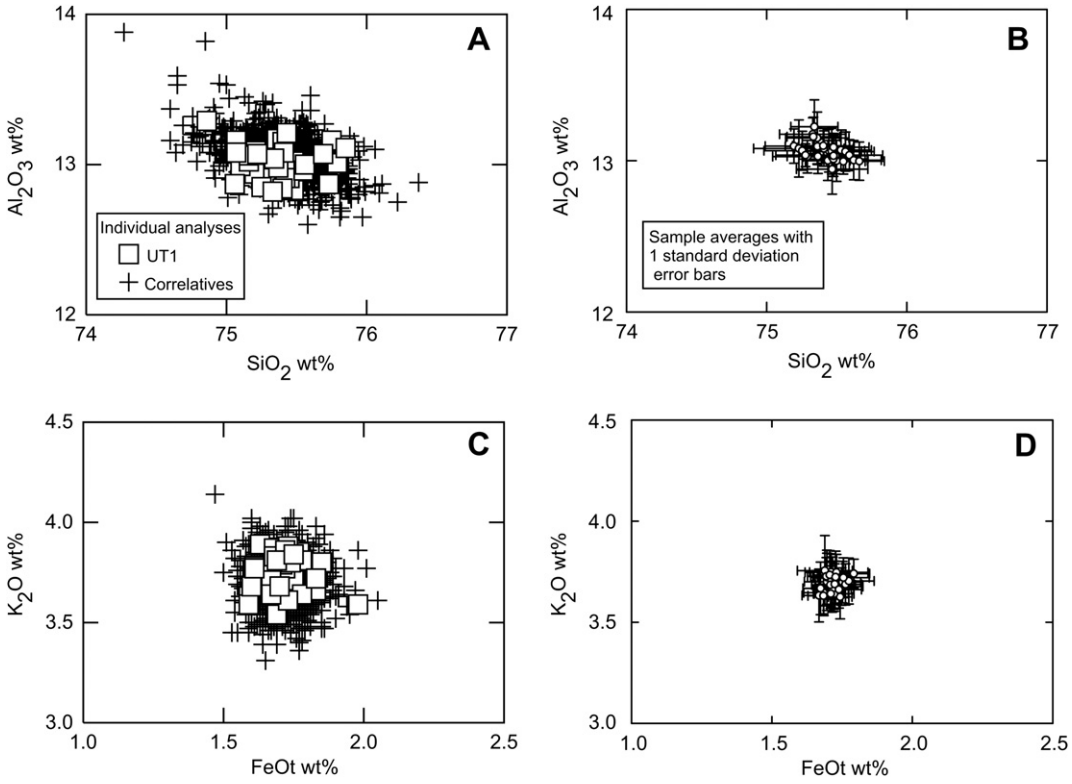

Fig. 2. Bivariate plots of Al_2O_3–SiO_2 and K_2O–FeOt showing individual glass-shard analyses of UT1 from the type locality ($n = 39$) and the OCt correlatives ($n = 885$) (A, C) and dispersion about site mean values (B, D). Data normalized to anhydrous basis. Additional plots are given in Fig. S1 (Supplementary Information).

shards from all 27 analyzed samples, when plotted on a NMORB-normalized incompatible element spider diagram, form a single coherent group of analyses (Fig. 3a, Table 2). This diagram shows enrichment in large ion lithophile elements and moderate depletions in Sr (the result of feldspar fractionation) and Ti (typical of arc-derived magmas and ilmenite/magnetite fractionation) (Fig. 3a). Chondrite normalized rare-earth element (REE) abundance plots show a sharp decrease from the light to middle REE ($La/Sm_{cn} \sim 4$) with an essentially flat profile from the middle to heavy REE at ~ 20–25 times chondrites. A marked negative Eu anomaly is exhibited by all samples, consistent with substantial feldspar fractionation during evolution of the parental magma (Fig. 3b). The glass geochemistry and petrography of OCt indicate that it belongs to the Type I group of Alaskan/Yukon distal tephra beds (Preece et al., 1992). Glass shards are dominantly clear, bubble-wall fragments with lesser mounts of pumice, although the latter is more common in samples from SW Alaska. Major mineral phases are plagioclase feldspar, hypersthene, augite, titanomagnetite and ilmenite, and trace amounts of amphibole, sanidine, biotite, apatite and zircon may also be present.

Trace-element variation between samples is better explored on bivariate plots (Fig. 4). In all cases, these data plot as a coherent cluster spanning only a limited range of concentrations (typically about ± 10% of the mean concentration). Linear trends are observed in several of the element-element pairs (e.g. U–Th, Zr–Rb) which are consistent with a small amount of magmatic evolution caused by fractional crystallization of feldspar, which has low distribution coefficients for these elements (Rollinson, 1993; Pearce et al., 2002, 2004). The small tail towards higher Sr (concentrations > 150 ppm, Fig. 4c) most probably reflects the inability to separate a small amount of feldspar from these glass concentrates and is reflected in the slightly higher RSD for Sr in the OCt samples (see Table 2). The strong correlations exhibited by many incompatible element pairs (Fig. 4) give single populations for ratios such as Zr/Y and U/Th. Thus, the trace-element data are consistent with all samples being derived from a single large eruption from a slightly compositionally zoned/fractionated magma.

Titano-magnetite compositions are dominated by a population with a TiO_2 content of ~9.4 wt.% (Fig. 5a, Table 4). A few crystals have higher and some lower TiO_2 contents (UT1, UA1124, UT1718, UT1805, and UT1816; Supplementary Table 2). Some of these outliers may be contaminants, others may be inherited from earlier magma batches. Ilmenite compositions cluster at ~ 43 wt.% TiO_2 (Fig. 5b, Table 5). The magmatic temperature and oxygen fugacity can be estimated from the composition of coexisting titano-magnetite and ilmenite provided they are in chemical equilibrium. The average titano-magnetite and ilmenite compositions in OCt samples from each site were evaluated for chemical equilibrium using the method of Bacon and Hirschmann (1988) and the temperature and oxygen fugacity of the magma were estimated using the method of Ghiorso and Evans (2008). Old Crow tephra samples are tightly clustered between 866 and 885 °C and from 0.78 to 0.87 log units above the Ni–NiO buffer (Table 6). Thus, both the titano-magnetite and ilmenite compositions, and the temperature and fugacity estimates are consistent with equilibration of the Fe–Ti oxides in a single magma prior to eruption. Typically, in a series of closely-spaced eruptions from the same source, variables such as temperature and oxygen fugacity of the magma change from one eruption to the next. This is due in part to zonation and movements of the magma body as well as ongoing petrologic processes within it. Examples of compositional, thermal, and oxygen fugacity variability of tephra beds produced by multiple, closely-spaced eruptions from the same volcano in Alaska and

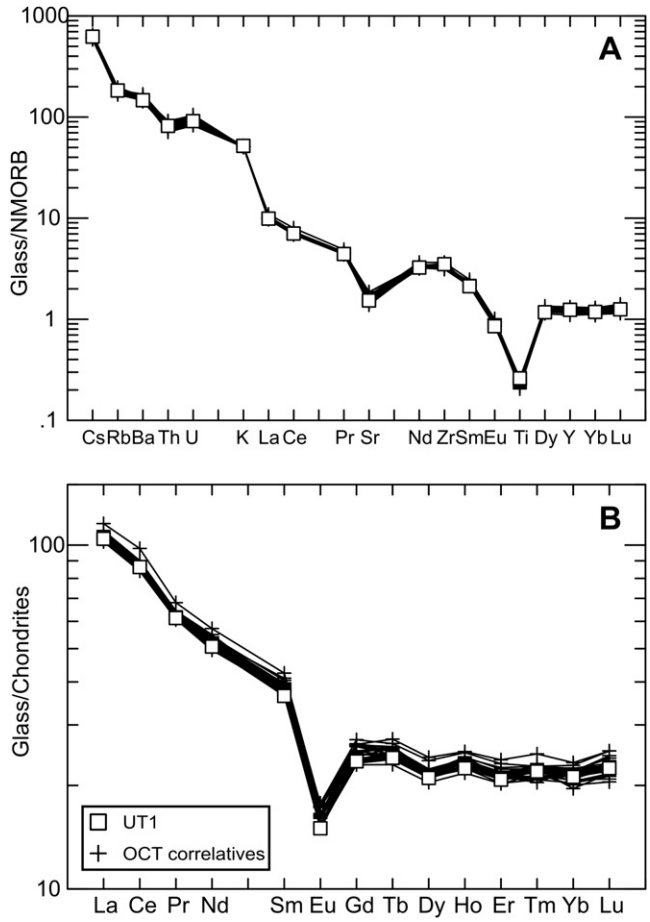

Fig. 3. (A) Spider diagram of type locality UT1 and OCt correlatives. Trace-element composition of glass shards normalized to NMORB composition of Sun and McDonough (1989). (B) Chondrite-normalized rare-earth element profile for UT1 and OCt correlatives. Chondrite values from Sun and McDonough (1989).

Yukon include White River Ash from Mount Churchill (Lerbekmo et al., 1975; Richter et al., 1995) and the Sheep Creek tephra beds, which probably come from Mount Drum, Alaska (Westgate et al., 2008).

4.2. Evidence for multiple eruptions?

We have presented a large body of data that favours OCt as the consequence of a single cataclysmic eruption rather than being the product of several events, closely spaced in time. However, field evidence at a few sites is suggestive of the latter scenario and so needs to be addressed. At site 10 on the Koyukuk River (Fig. 1), 5 cm of massive OCt is overlain by several thin tephra beds intercalated with lacustrine silt, totalling about 25 cm in thickness (Fig. 6a). Do these thin tephra beds indicate several discrete eruptions, or are they due to subaerial processes reworking tephra on the adjacent watershed and sporadically flushing it into the lake? Samples of four thin tephra beds were collected and analyzed for the major- and trace-element content of their glass shards, as well as major-element composition of titano-magnetite and ilmenite (Fig. 7a; Tables 2–5; Supplementary Tables 1–3). These data are consistent with all samples being derived from the same magma batch, favouring a reworked origin for the thin tephra beds. Primary emplacement of the latter as thin airfall tephra deposits would require many large-magnitude eruptions because the Koyukuk locality is distant from volcanoes of the eastern Aleutian Arc and the Wrangell volcanic field (Fig. 1). We have seen no evidence supporting this idea elsewhere in eastern Beringia, although we acknowledge that smaller eruptions involving proximal deposition of tephra may well have occurred shortly before and/or after the Old Crow event.

Stratification of OCt at site 12, near Halfway House, Alaska, could be interpreted as evidence for multiple eruptions because the lower 14 cm consists of four sub-horizontal, fining-upwards layers. The overlying 16 cm of tephra is reworked (UT901) and includes pods with slightly different colours and/or textures (UT899, UT900; Fig. 6b). Major- and trace-element glass analyses of these graded beds (Supplementary Table 1; Preece et al., 1999) show very little variation (Fig. 7b) and are within the compositional range expressed by OCt at all the other sites. This stratification more likely is a primary sedimentary feature reflecting textural variations in the plume. The absence of intervening sediment supports this view.

Organic-rich silts close to OCt in different parts of the Eva II exposure, near Fairbanks, Alaska (site 13, Figs. 1 and 8) do not yield the same pollen assemblage (Muhs et al., 2001) and could be interpreted as evidence for multiple OCt beds. In some places, spruce wood in organic-rich sediments of the interglacial Eva Forest Bed occurs below or at the same level as OCt. Elsewhere in this exposure, OCt is associated with sediments deposited under much cooler conditions, the pollen indicating a sedge-dominated tundra with willows. Again, analyses of glass, titano-magnetite, and ilmenite (Fig. 9; Tables 2–5; Supplementary Tables 1–3) argue for a single eruptive unit. The varied pollen data from sediments close to OCt can be readily explained by deformation of OCt and nearby sediments due to extensive cryoturbation and collapse due to melting ice masses.

5. Comparison with compositionally similar tephra beds and pumice clasts

In order to emphasize the homogeneity of Old Crow tephra, we compare it with compositionally similar tephra beds in eastern Beringia. Our tephra database was searched for tephra samples whose major-element composition is similar to OCt. The search parameters were set relative to the average composition of OCt (Table 3) as follows: $SiO_2 \pm 1.5$ wt. %, $Al_2O_3 \pm 1.0$ wt. %, $FeOt \pm 0.5$ wt. %, $CaO \pm 0.5$ wt. %, $Na_2O \pm 1.0$ wt. %, and $K_2O \pm 0.5$ wt. %. Three tephra beds and three pumice clasts returned as being similar in composition to OCt: Dawson, DL, Togiak tephra beds, and three isolated pumice clasts, C2 pumice 1, C2 pumice 2, and C2 pumice 3. Dawson tephra is widespread across Alaska and Yukon and correlates to the C2 caldera-forming eruption of Emmons Lake volcanic center (Fig. 1; Westgate et al., 2000; Mangan et al., 2003). The three C2 pumice samples are large clasts collected from the flanks of Trader Mountain, located on the SW Alaska Peninsula about 15 km north of the caldera rim of Emmons Lake volcanic center (ELVC) (F. Wilson, written communication, 1990). Given their locations and compositional similarity to Dawson tephra, these pumice clasts are presumed to be part of the C2 caldera-forming eruption of ELVC (Mangan et al., 2003, 2009). Each of the presumed C2 pumice clasts has a slightly different composition and only C2 pumice 1 is the same as Dawson tephra. DL is known from one section in the Kulukak Bay area in SW Alaska (58° 55.9'N, 159° 41.34'W; sample provided by W. Manley). Togiak tephra is also from SW Alaska and is described in Kaufman et al. (2001b). Average major- and trace-element contents of glass shards belonging to these tephra beds and pumice clasts are listed in Table 7 and temperature and oxygen fugacity estimates from Fe–Ti oxide equilibria are given in Table 8.

Elemental and ratio scatter plots of glass shards for OCt and the compositionally similar tephra beds and pumice clasts are plotted

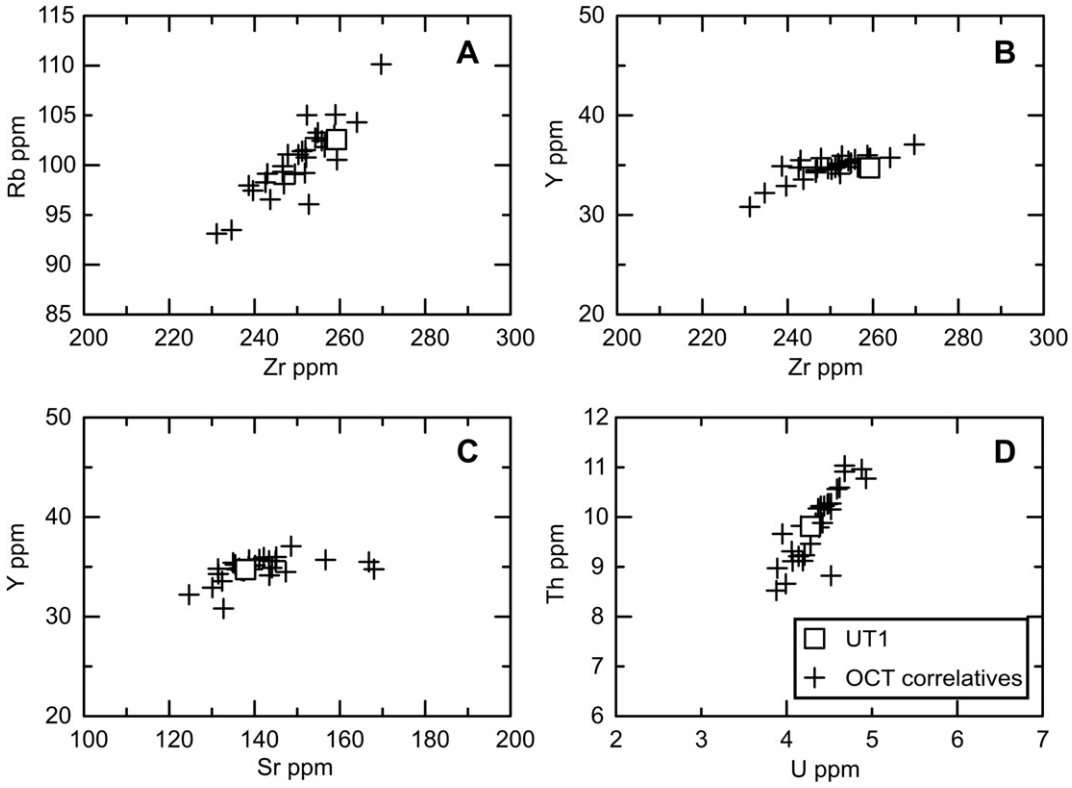

Fig. 4. Bivariate plots showing Rb–Zr, Y–Zr, Y–Sr, and Th–U for UT1 and OCt correlatives.

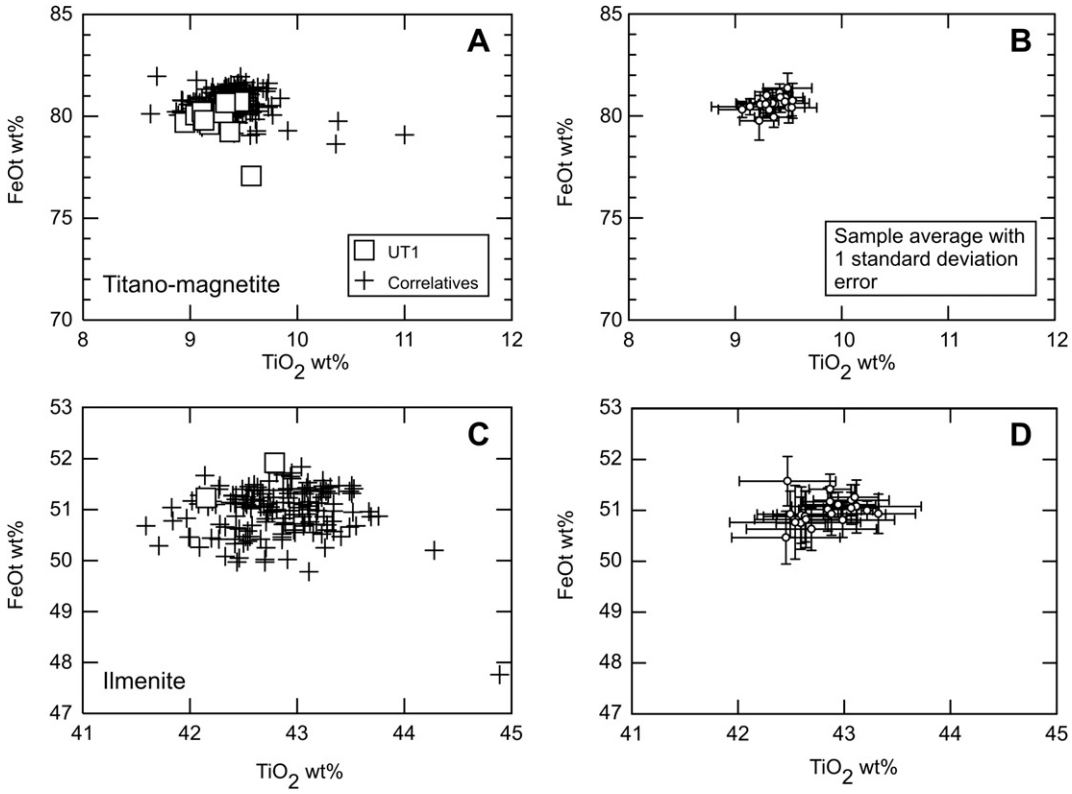

Fig. 5. Bivariate plots of FeOt–TiO_2 for titano-magnetite ($n = 261$) and ilmenite ($n = 158$) compositions of UT1 and OCt correlatives (A, C) and dispersion about site mean values (B, D).

Table 6
Geothermometry estimates for Old Crow tephra samples.

Site #	Site name	Temperature °C (Fe–Ti exchange)	$\log_{10} fO_2$ (ΔNNO)
26	Type locality	878	0.87
2	Togiak Bay	873	0.8
3	Hagemeister Island	871	0.78
4	Holitna	870	0.79
5	Imruk Lake	873	0.83
6	Baldwin Peninsula	878	0.8
8	NK29A	868	0.81
9	Hogatza Mine	873	0.82
10	Ky-11	872	0.81
11	Palisades	879	0.83
12	Halfway House	885	0.84
13	Eva	871	0.82
18	Birch Creek	870	0.82
19	Chester Bluff	868	0.81
20	Mile 293	873	0.81
21	Mirror Creek	873	0.81
22	Thistle (UT1805)	875	0.81
22	Thistle (UT1816)	875	0.78
22	Thistle (UT1823)	866	0.82
24	Caribou Creek 2	881	0.85
25	Klondike	872	0.84

Notes: Geothermometry estimates of titano-magnetite and ilmenite pairs using the method of Ghiorso and Evans (2008) and software from http://www.ofm-research.org. All data fulfill the equilibrium conditions of Bacon and Hirschmann (1988). Results are based on the average composition of titano-magnetite and ilmenite.

in Fig. 10. Many of these units have overlapping fields with respect to their major-element composition and together form a continuum in composition (Fig. 10a). On the other hand, OCt forms a discrete group on most of the trace-element scatter plots (Fig. 10b, c), although there is overlap for some trace elements with DL (Fig. 10d). Old Crow tephra and C2 pumice 2 have very similar titano-magnetite and ilmenite compositions (Fig. 10e, f) and estimates of their temperature and oxygen fugacity group closely together (Fig. 10g). Dawson, DL, and C2 pumice 1 tephra have comparable temperatures but lower estimated oxygen fugacity (Fig. 10g). Rare-earth element profiles of OCt and the geochemically similar tephra beds and pumice clasts are plotted in Fig. 11. They all show LREE enriched profiles with negative Eu anomalies but none shows REE concentrations coincident with OCt. Dawson, DL, and C2 pumice samples have shallower REE profiles with La/Lu_{cn} between 2.5-3.0 (Fig. 10b, c) whereas OCt

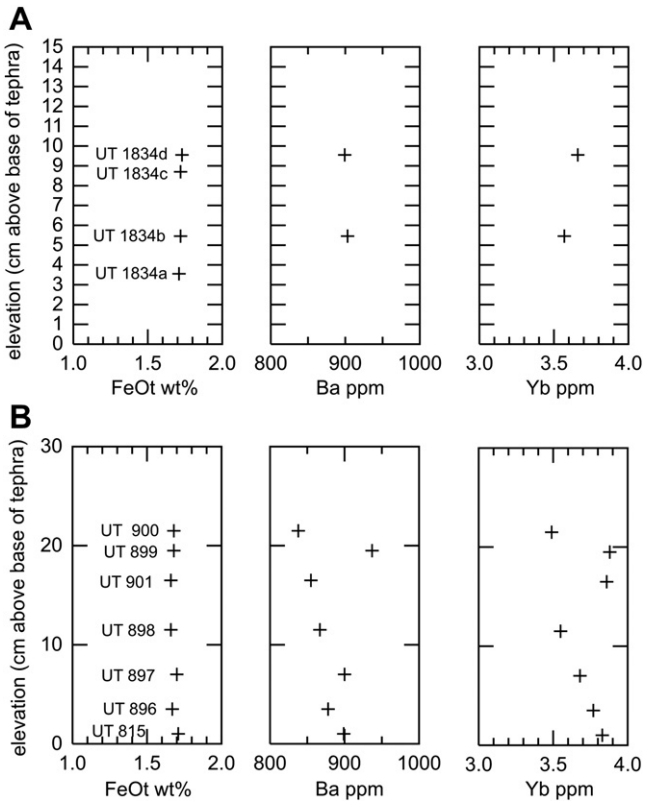

Fig. 7. Scattergrams showing vertical variation in composition of glass shards for samples from (A) site 10 on the Koyukuk River, and (B) Halfway House (site 12). Small sample size precluded trace-element analysis of two of the four samples taken at the Koyukuk site.

samples have La/Lu_{cn} between 4.0-4.7 (average 4.32 ± 0.18). The Togiak deposit has La/Lu_{cn} similar to the highest values exhibited by OCt (~4.7), but REE concentrations are a factor of ~ 2 lower in the Togiak sample (Fig. 11, Table 7).

Statistical distance measures have been applied elsewhere to test the possibility that silicic tephra samples are different (Pearce et al., 2004, 2008; Denton and Pearce, 2008). The statistical distance measure was developed by Perkins et al. (1995, 1998) and

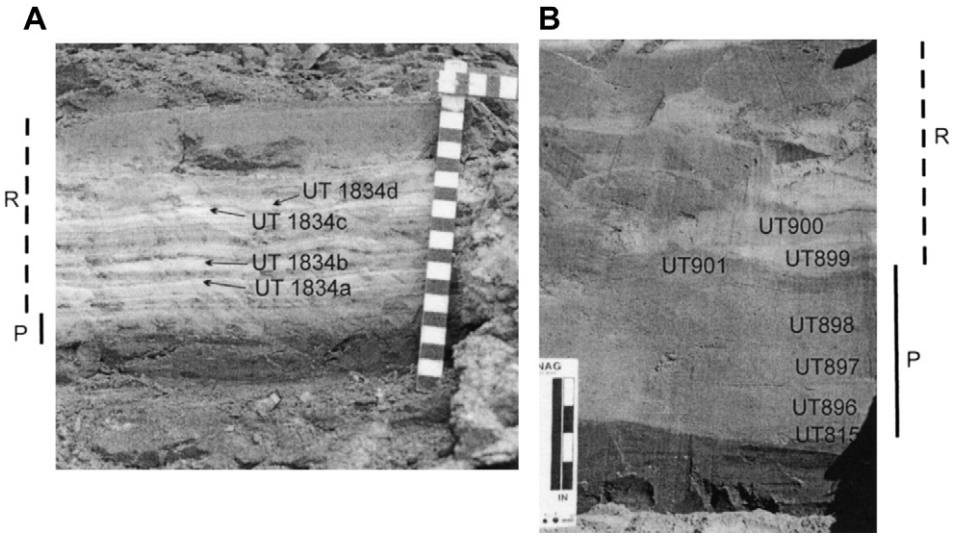

Fig. 6. Old Crow tephra at (A) Koyukuk River Ky-11 (site 10) and (B) Halfway House (site 12) showing location of samples analyzed in this study. Photograph 6A courtesy of T. Hamilton. Both scales are in inches. P = primary tephra, R = reworked tephra.

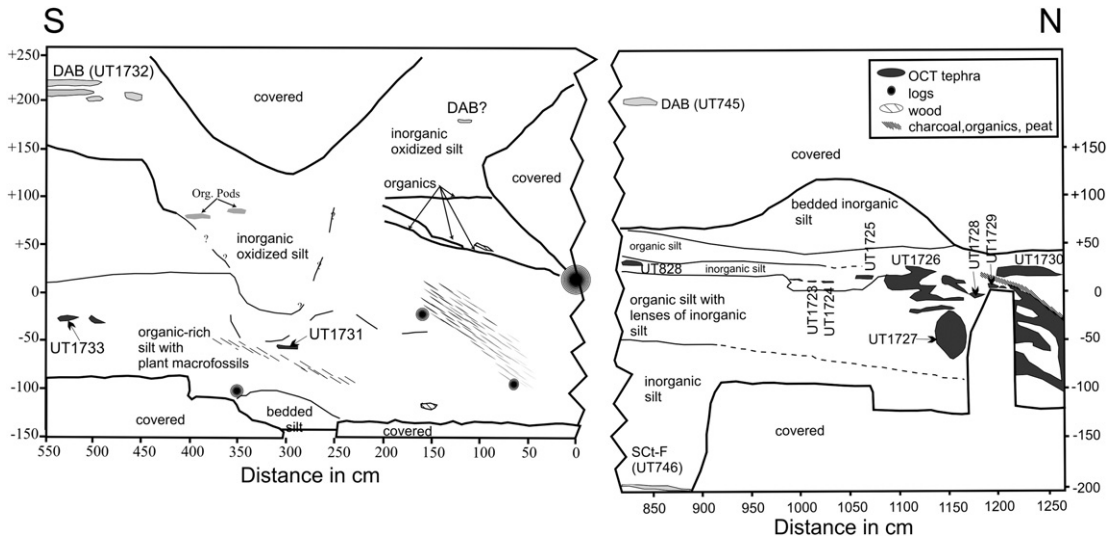

Fig. 8. Stratigraphy of loess and tephra deposits at Eva II, Fairbanks, Alaska (based on mapping by N. Bigelow, August, 2000, and modified by S. Preece). Elevation and horizontal distance is in centimetres measured from a prominent log at the centre of the exposure. Dome Ash Bed (DAB) sample UT745 and OCt sample UT828 were collected in 1987 and elevations are extrapolated based on field measurements taken in 1987 and 1989. All other DAB and OCt samples were collected in August, 2001. Samples UT1723, UT1724, UT1725, UT1726, UT1728, and UT1729 have the same petrographic features as the analyzed OCt samples.

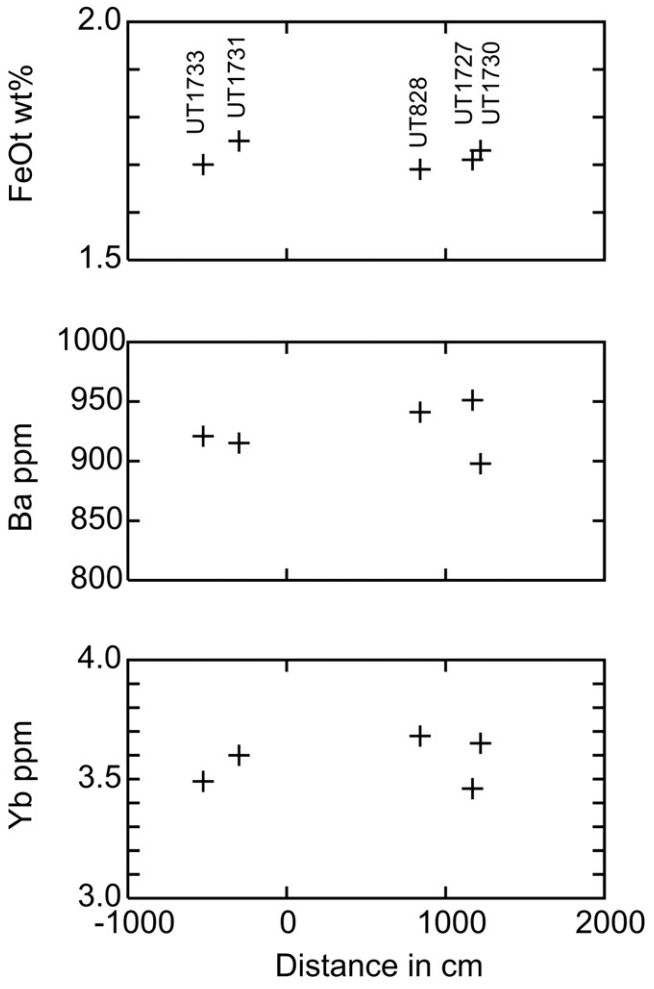

Fig. 9. Scattergrams showing variation in composition of glass shards for samples across the Eva II section. Horizontal distance is measured from the large log in the exposure, documented by Péwé et al. (1997) and shown in Fig. 8.

has been used here to investigate any differences in the OCt glass shard major-element data. Statistical distance is calculated as:

$$D^2 = \sum_{(k=1)}^{n} (x_{k1} - x_{k2})^2 / \left(\sigma_{k1}^2 + \sigma_{k2}^2\right) \quad (1)$$

where n is the number of elements used in the comparison, x_{k1} and x_{k2} are the concentrations of the kth element in the first and second samples, and σ_{k1} and σ_{k2} are the standard deviations of the determinations of the kth element in each sample. Providing the data are normally distributed, the value of $D^2_{\text{calculated}}$ has a Chi-squared distribution amongst compositionally identical samples (Perkins et al., 1995). If the calculated statistical distance between two samples exceeds a critical value, D^2_{critical}, for a comparison of a given number of elements (the degrees of freedom, F), at a particular confidence interval (e.g. 99%), the two samples can be considered different. Thus, to be 99% certain that two samples are different $D^2_{\text{calculated}}$ would have to exceed the D^2_{critical} value of 21.67 when comparing 9 elements in the samples. The probability that the samples are different decreases as the calculated statistical distance between samples becomes smaller. Thus, for $F = 9$, a $D^2_{\text{calculated}} < 2.09$ indicates that the probability that the samples are statistically different is <1%. Compositionally identical samples would have $D^2 = 0$. The matrix of $D^2_{\text{calculated}}$ for all pairs of OCt correlatives is presented in Table 9 for nine major-elements determined by EPMA (MnO and H_2O_d have been excluded). All of the OCt pairs have a $D^2_{\text{calculated}}$ below 6 with most having $D^2_{\text{calculated}} < 2$, indicating the probability of the supposed OCt correlatives being different is very low. Pairs of OCt with Dawson, DL, Togiak, C2 pumices 1, 2, and 3 all have $D^2_{\text{calculated}} > 23$ and are easily differentiated from OCt. This can be seen graphically by performing single linkage cluster analysis on the matrix resulting from use of the statistical distance measure of Perkins et al. (1995, 1998) (Fig. 12, Table 9). The cluster analysis was done using the Stata 10 software package; Microsoft Excel was used to calculate the statistical distance measure. The resulting dendrogram shows OCt occurrences tightly clustered and separate from the other tephra beds and pumice clasts.

Table 7
Tephra beds and pumice clasts with compositions similar to Old Crow tephra.

Unit	Dawson tephra		DL tephra		Togiak tephra		C2 pumice 1		C2 pumice 2		C2 pumice 3	
SiO_2	74.19	(0.29)	74.04	(0.10)	75.05	(0.20)	74.11	(0.20)	74.06	(0.16)	74.84	(0.39)
TiO_2	0.27	(0.08)	0.35	(0.05)	0.25	(0.08)	0.26	(0.08)	0.25	(0.10)	0.26	(0.07)
Al_2O_3	13.68	(0.15)	13.78	(0.08)	13.62	(0.10)	13.73	(0.13)	13.68	(0.10)	13.87	(0.20)
FeOt	2.05	(0.09)	1.85	(0.05)	1.70	(0.07)	2.08	(0.08)	2.01	(0.08)	1.39	(0.34)
MnO	0.07	(0.04)	0.05	(0.03)	0.05	(0.03)	0.08	(0.05)	0.06	(0.03)	0.04	(0.03)
CaO	1.26	(0.08)	1.39	(0.04)	1.40	(0.09)	1.25	(0.06)	1.29	(0.06)	1.06	(0.08)
MgO	0.21	(0.03)	0.26	(0.02)	0.23	(0.03)	0.22	(0.03)	0.22	(0.03)	0.11	(0.05)
Na_2O	4.43	(0.20)	4.29	(0.12)	4.08	(0.12)	4.39	(0.09)	4.56	(0.08)	4.41	(0.10)
K_2O	3.64	(0.11)	3.78	(0.06)	3.50	(0.11)	3.67	(0.09)	3.66	(0.11)	3.84	(0.11)
Cl	0.21	(0.04)	0.23	(0.04)	0.11	(0.03)	0.22	(0.04)	0.21	(0.05)	0.17	(0.05)
$H2O_d$	2.15	(1.63)	2.83	(1.32)	3.48	(1.22)	3.73	(1.48)	3.56	(0.69)	4.28	(1.94)
n	329		10		36		14		19		18	
Sc	5.11	(0.17)	4.24	(0.37)	2.97	(0.01)	7.62		nd		nd	
Rb	85.0	(9.0)	86.3	(4.6)	120	0	70.2		114	(7)	104	(8)
Sr	73	(7)	113	(30)	98	0	180		121	(17)	93	(20)
Y	39.6	(2.2)	30.6	(0.4)	17.2	(0.5)	45.9		66.2	(7.0)	51.6	(4.1)
Zr	299	(29)	248	(9)	147	(4)	259		446	(31)	337	(24)
Nb	7.31	(1.15)	6.30	(0.58)	3.64	(0.09)	6.07		13.0	(2.0)	9.72	(1.01)
Cs	5.13	(0.45)	5.42	(0.14)	8.74	(0.00)	4.02		7.22	(0.74)	6.43	(0.67)
Ba	920	(52)	883	(35)	848	(5)	721		1140	(95)	965	(62)
La	19.7	(0.8)	18.2	(0.4)	16.1	(0.1)	19.9		33.1	(2.8)	27.5	(1.7)
Ce	40.6	(3.3)	34.9	(0.3)	28.9	(0.1)	47.6		64.1	(4.9)	54.9	(6.1)
Pr	5.86	(0.33)	4.98	(0.10)	3.76	(0.14)	5.85		9.02	(0.74)	7.11	(0.51)
Nd	23.4	(1.5)	18.7	(0.7)	13.7	(0.1)	25.1		37.6	(3.8)	31.5	(3.7)
Sm	5.82	(0.51)	4.47	(0.26)	3.19	(0.09)	6.94		9.61	(1.69)	8.29	(1.31)
Eu	0.95	(0.06)	0.86	(0.09)	0.66	(0.08)	1.08		2.01	(0.44)	1.23	(0.32)
Gd	6.33	(0.53)	5.01	(0.08)	3.10	(0.06)	5.87		10.15	(1.23)	7.96	(1.11)
Tb	1.07	(0.07)	0.85	(0.01)	0.51	(0.00)	1.14		1.62	(0.27)	1.27	(0.20)
Dy	6.76	(0.55)	5.29	(0.04)	2.96	(0.06)	6.93		9.89	(1.17)	8.52	(0.97)
Ho	1.46	(0.19)	1.09	(0.00)	0.61	(0.01)	1.71		2.14	(0.27)	1.82	(0.26)
Er	4.31	(0.48)	3.16	(0.03)	1.90	(0.08)	4.63		7.00	(0.76)	5.61	(0.74)
Tm	0.76	(0.08)	0.59	(0.05)	0.28	(0.02)	0.64		1.00	(0.23)	0.86	(0.15)
Yb	4.64	(0.53)	3.59	(0.13)	1.97	(0.01)	4.21		7.28	(0.57)	6.07	(0.56)
Lu	0.80	(0.07)	0.64	(0.01)	0.32	(0.01)	0.67		1.22	(0.18)	0.95	(0.14)
Hf	8.43	(0.77)	7.32	(0.11)	4.36	(0.14)	6.93		12.02	(1.41)	10.03	(1.02)
Ta	0.50	(0.16)	0.40	(0.17)	0.34	(0.08)	0.45		0.92	(0.17)	0.65	(0.12)
Th	7.50	(0.70)	7.08	(0.27)	10.70	(0.49)	6.41		11.55	(0.94)	9.70	(1.47)
U	4.02	(0.26)	3.95	(0.33)	6.56	(0.05)	3.02		4.71	(0.51)	3.85	(0.77)
n	9		2		2		1		16		15	

Notes: Standard deviation in brackets; FeOt, total Fe as FeO; n, number of analyses. Average composition (wt. %) based on the following samples: Dawson (UA581, UA582, UA68, UA69, UT1056, UT1057, UT1059, UT1061, UT11, UT12, UT1488, UT1504, UT1593, UT1611, UT1612, UT1614, UT1626, UT1635, UT1776, UT1781, UT18, UT1910, UT20, UT2214, UT361, UT540, UT719), DL (UT1433), Togiak (UT1411), C2 pumice 1 (UT707), C2 pumice 2 (UT706), and C2 pumice 3 (UT709). All trace element analyses performed at Aberystwyth University. Solution ICP-MS analysis following $HF/HClO_4$ digestion was used for Dawson (average of UA582, UT1593, UT1611, UT1612, UT1635, UT 540, see Westgate et al., 2000; Pearce et al., 2004); DL (UT1433, Pearce et al., 2004); Togiak (UT1411, Pearce et al., 2004), C2 pumice 1 (UT707, this study). LA-ICP-MS was used for C2 pumice 2 (UT706) and C2 pumice 3 (UT709) using a Coherent MicroLas Excimer laser ablation system coupled to a Thermo Finnegan Element 2 sector field ICP-MS, following methods described in Pearce et al. (2004, 2007). nd = not determined.

Table 8
Geothermometry estimates for tephra beds and pumice clasts with a composition similar to Old Crow tephra.

Tephra bed	Temperature °C (Fe–Ti exchange)	$\log_{10} fO_2$ (ΔNNO)
Dawson, UT1635	858	−0.48
Dawson, UT540	875	−0.43
DL, UT1433	859	0.19
DL, UT1433	872	0.14
C2 pumice 1, UT707, 7ab	893	−0.08
C2 pumice 2, UT706, 7ab	871	0.85
C2 pumice 2, UT706, 10ab	901	0.79
C2 pumice 2, UT706, 11ab	881	0.75
C2 pumice 2, UT706, 12ab	887	0.81
C2 pumice 2, UT706, 13ab	873	0.73

Notes: Geothermometry estimates of titano-magnetite and ilmenite pairs using method of Ghiorso and Evans (2008) and software from http://www.ofm-research.org. All data fulfills the equilibrium conditions of Bacon and Hirschmann (1988). Dawson and DL estimates are based on the average composition of titano-magnetite and ilmenite. C2 pumice 1 and pumice 2 are based on individual analyses of titano-magnetite and ilmenite that are in physical contact with one another. Magnetite and ilmenite compositions for these samples are given in Supplementary Tables 2 and 3.

The statistical distance measure of Perkins et al. (1995, 1998) is not easy to apply to the trace-element analyses of single samples of the OCt correlatives by solution nebulisation ICP-MS because it is difficult to get a realistic measure of analytical error/precision for these materials. Multiple preparations and analyses of homogeneous materials give relative errors of <5% (see data for the USGS reference materials QLO-1 and RGM-1 in Table 2 and Pearce et al., 2004), but the lack of a sufficient mass of separate from the OCt samples prevented multiple analyses of these samples. The use of the error derived from the reference material analyses in any distance calculations would not be appropriate for the glass separates because it would not account for any natural heterogenity within a sample which would be identified only by different preparations of the same deposit. To overcome this, cluster analysis can be used to examine the structure of large trace-element data sets where the Euclidean distance is calculated between samples (e.g. Preece et al., 1999). This measure does not have a Chi-squared distribution and cannot be used to predict how the samples differ from one another. Single-linkage cluster analysis was performed on the matrix calculated from the trace-element Euclidean distance between samples and the results are presented as a dendrogram (Fig. 13). Euclidean distance calculations and cluster analysis were

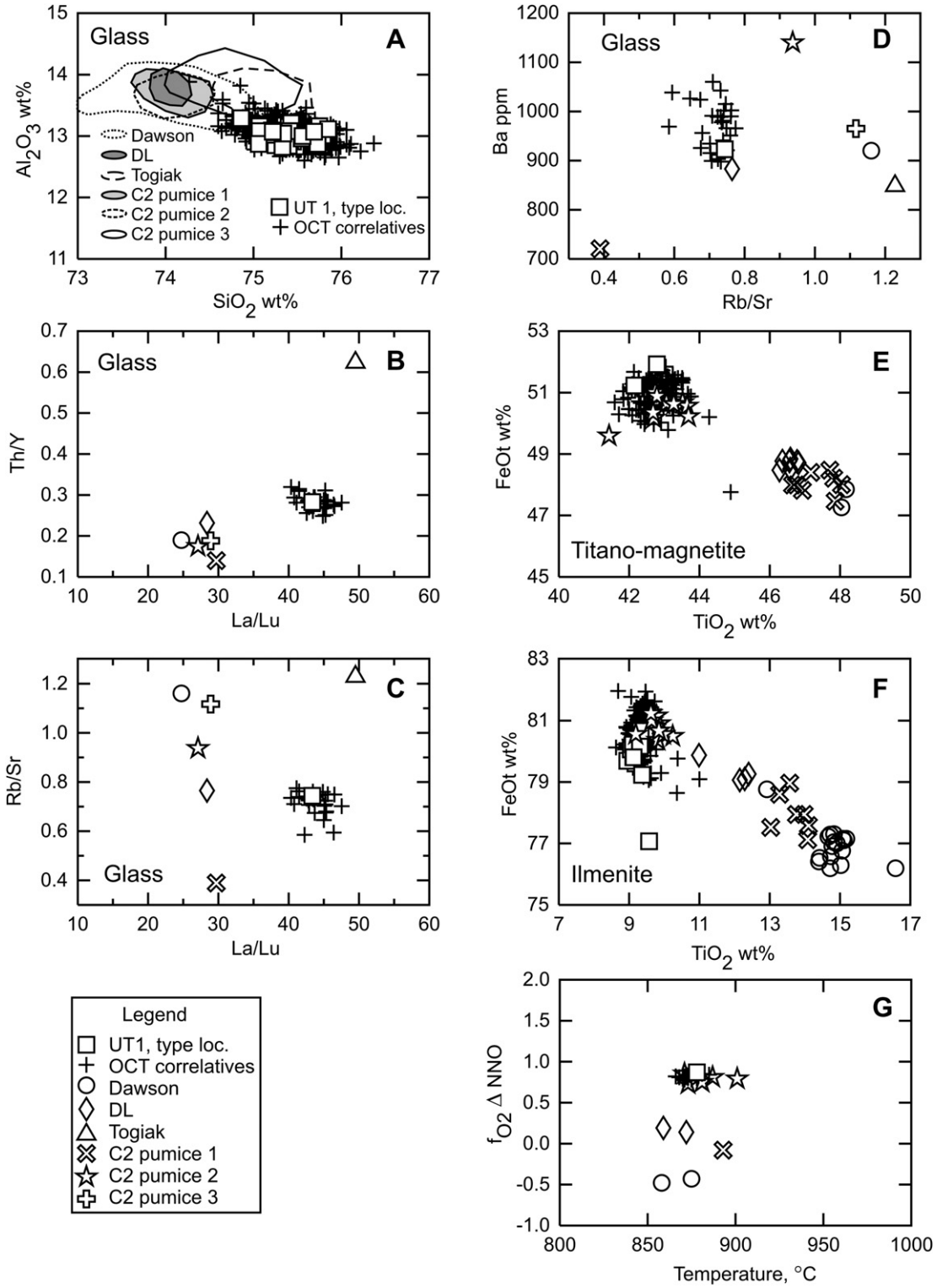

Fig. 10. Scattergrams of OCt samples and the compositionally similar tephra beds, Dawson, DL, Togiak, and C2 pumice clasts (samples 1, 2, and 3). (A) Al_2O_3–SiO_2 plot of individual glass shards of UT1 and OCt correlatives compared to fields for the compositionally similar tephra beds. Trace-element ratio scattergrams (B) Th/Y–La/Lu, (C) Rb/Sr–La/Lu, and (D) Ba–Rb/Sr, show tight clustering of OCt samples, which are clearly separated from the other samples with the exception of DL in (D). In scattergrams of titano-magnetite (E) and ilmenite grains (F), OCt and C2 pumice 2 samples overlap. (G) Plot of oxygen fugacity versus temperature for OCt and the compositionally similar tephra beds and pumice clasts. Oxygen fugacity is measured in log units from the Ni–NiO buffer (ΔNNO) and calculated using method of Ghiorso and Evans (2008). Old Crow tephra and C2 pumice 2 samples formed under similar conditions, while Dawson, DL, and C2 pumice 1 tephra deposits formed at similar temperatures but lower oxygen fugacities.

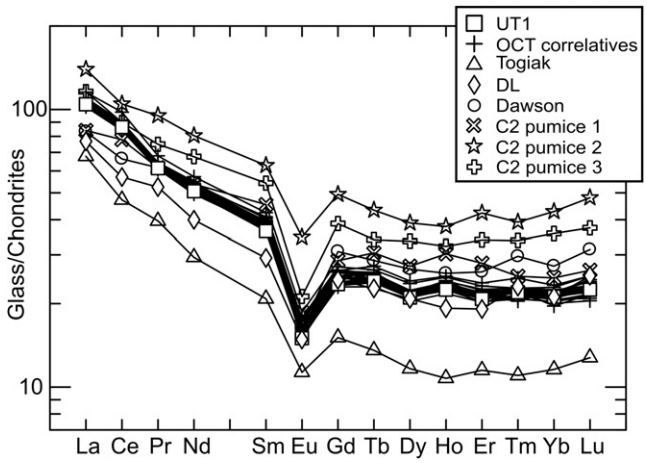

Fig. 11. Chondrite-normalized rare-earth element profiles for OCt, Dawson, DL, Togiak tephra beds, and C2 pumice 1, 2, and 3. Chondrite values from Sun and McDonough (1989).

done using the Stata 10 software package. OCt samples are tightly clustered together at low joining distances, while the other six compositionally similar tephra beds and pumice clasts join the OCt samples at higher joining distances.

Together, the combination of graphical and statistical techniques demonstrates that OCt can easily be distinguished from the six compositionally similar tephra beds and pumice clasts. In addition, trace-element cluster analysis along with Fe-Ti oxide data do not allow OCt to be divided into subgroups that could relate to multiple eruptions from a single source.

6. Age

We recently summarized the evidence bearing on the age of OCt, noting a glass fission-track (FT) age of 131 ± 11 ka and a paleoecological context supporting deposition during the MIS 6 to MIS 5 transition, that is, prior to growth of the last interglacial boreal forest in eastern Beringia (Péwé et al., 2009). The age monitor in our FT dating studies is the Moldavite tektite glass, our calibration being based on an $^{40}Ar/^{39}Ar$ plateau age of 15.21 ± 0.15 Ma (Staudacher et al., 1982). More recent and precise age determinations have shown that the Moldavite glass is younger. The average $^{40}Ar/^{39}Ar$ age of 7 individual specimens from southern Bohemia and Moravia is 14.34 ± 0.08 Ma (±1σ) (Laurenzi et al., 2003, 2007). This result has necessitated a recalibration of our glass FT dating method, which now gives mean age estimates that are ~5% younger – a value that is within the error due to counting statistics for most Pleistocene tephra beds. Table 10 shows that the new calibration scheme does give glass FT ages that are closer to the $^{40}Ar/^{39}Ar$ age of some reference glasses (Balestrieri et al., 1998). It also gives the revised ages for the four OCt samples, the weighted mean of which is 124 ± 10 ka. Given the ~ 8% error associated with the FT age of OCt, a more precise definition of its age can only be assessed in conjunction with stratigraphic and paleoecological data. Old Crow tephra always underlies the last interglacial sediments when both are present (Table 1) with the possible exception of the Hogatza Mine exposure (site 9, Fig. 1) where a peat bed underlies OCt. However, this section has not received much study and the composition of OCt there is indistinguishable from OCt elsewhere. In this context, new and detailed paleoecological studies of a vegetation surface buried by Old Crow tephra at the Palisades section on the Yukon River (site 11, Fig. 1) indicate it fell on a shrub-tundra environment, lacking arboreal pollen, during late MIS 6 time (Reyes et al., 2010), corroborating the conclusions reached by Péwé et al. (2009).

7. Volume estimate of tephra erupted

Several realities work against an accurate definition of the total volume of tephra erupted. Old Crow tephra was deposited over most of Alaska and much of Yukon yet only 27 occurrences are known, and most of these are distal and reworked (Fig. 1, Table 1). Further, the source caldera is unknown, although it is likely somewhere in the eastern Aleutian arc. Under these circumstances, drawing isopachs over the fallout area is a precarious task. Nonetheless, we have attempted to do this and have taken a conservative approach in interpreting the primary thickness of the tephra at each site (Fig. 6). The isopach map is shown in Fig. 14 and suggests a dispersal axis trending to the northeast. An approximation of the thickness of OCt at its source was determined by the method of Pyle (1989). Using the 5, 10, 15, and 30 cm isopachs, a straight line relationship was obtained on a plot of the natural logarithm of thickness (ln T) versus the square root of the corresponding isopach area (√A). Extrapolating this line to √A = 0 gives a thickness of 50 cm (Fig. 15).

A minimum volume was estimated by a graphical technique (Froggatt, 1982). A 100 x 100 km grid was drawn over the fallout area using a map of eastern Beringia with an equal-area projection. The area within each isopach (A) was then determined by counting the number of 100 × 100 km squares it contained. The results are shown in Table 11. The area of each isopach annulus can then be calculated by subtracting the smaller area from the larger (i.e. $A_{10cm}-A_{15cm}$) and its volume determined by using a mean thickness of 0.6 of the value of the bounding isopachs based on the exponential decay of thickness (i.e. for isopachs 10 cm and 15 cm, 13 cm was used). Total volume within the outermost (minimum) isopach is then calculated by summing the volume of each annulus. In this way, we obtained a minimum bulk tephra volume (i.e. within the 1 cm isopach) of 215 km^3.

As a check on this volume estimate, we used Garmin MapSource software to estimate the area within the isopachs and obtained results very similar to those of the graphical method (Table 11). The minimum bulk tephra volume by this approach is estimated at 220 km^3.

Fierstein and Nathenson (1992) provide another way of determining bulk tephra volume, in this case the total volume of tephra erupted. Their expression for calculating total bulk tephra volume is:

$$V = 2T_o/k^2 \quad (2)$$

where T_o is the extrapolated thickness at A (area) = 0 and k is the slope of the line on a ln T versus $A^{½}$ plot. In our case, T_o = 50 cm and k = 0.0021 (Fig. 15). These values give a volume of 225 km^3. Although these different methods are in broad agreement, we emphazise again the uncertainty inherent in this exercise given the limited controls on isopach thickness over such a large area. Hence, these results should be considered as tentative.

8. Source

The source of OCt is unknown, but the distribution of OCt sites, isopach thicknesses, and general coarsening of samples towards the southwest all suggest that it is located in the southwestern part of the eastern Aleutian arc, possibly the Emmons Lake

Table 9
Results of statistical distance measure, D^2, for OCt samples and other tephra beds and pumice clasts with similar chemistry calculated using SiO_2, TiO_2, Al_2O_3, FeO, MgO, CaO, Na_2O, K_2O and Cl.

	UT1 Type loc.	Goodnews Bay	Togiak Bay	Hagemeister Island	Holitna	Imruk Lake	Baldwin Pen.	NK26B	NK29A	Hogatza Mine	Ky-11	Palisades	Halfway House	Eva	West Dawson	Birch Hill	Sheep Ck. Valley	Gold Hill
UT1 Type loc.	0.00																	
Goodnews Bay	2.57	0.00																
Togiak Bay	1.55	0.44	0.00															
Hagemeister Is.	1.66	0.93	0.71	0.00														
Holitna	1.18	1.30	0.88	0.81	0.00													
Imruk Lake	1.95	0.99	0.91	1.40	1.52	0.00												
Baldwin Pen.	1.03	1.46	1.00	1.21	1.15	0.27	0.00											
NK26B	0.38	1.43	0.76	0.72	0.88	1.28	0.73	0.00										
NK29A	0.36	1.78	1.42	1.22	1.11	1.60	0.69	0.54	0.00									
Hogatza Mine	1.41	0.48	0.68	0.85	1.38	0.52	0.47	0.87	0.95	0.00								
Ky-11	0.37	1.89	1.28	0.92	0.60	2.01	1.28	0.32	0.47	1.50	0.00							
Palisades	1.96	2.40	1.57	3.66	2.72	1.63	1.64	2.64	2.15	1.44	2.91	0.00						
Halfway House	1.19	1.36	1.26	0.82	1.26	1.80	0.88	0.85	0.51	0.72	1.06	2.46	0.00					
Eva	0.78	0.86	0.77	0.34	0.54	1.28	0.64	0.47	0.31	0.46	0.50	2.06	0.22	0.00				
West Dawson	1.03	1.44	1.38	0.73	0.39	1.60	1.07	0.69	0.83	1.65	0.44	3.54	1.19	0.57	0.00			
Birch Hill	1.27	1.75	1.83	0.72	0.72	2.65	1.84	0.93	1.20	1.81	0.43	4.62	1.14	0.62	0.49	0.00		
Sheep Creek	2.11	4.00	2.90	1.41	1.92	3.17	1.74	1.70	1.42	1.76	1.75	5.18	0.52	0.78	1.26	1.04	0.00	
Gold Hill	2.34	1.68	2.10	1.66	2.01	3.17	1.68	1.87	1.30	1.50	1.92	3.89	0.25	0.61	2.00	2.06	0.99	0.00
Birch Creek	1.66	2.97	1.63	1.16	0.71	2.10	1.15	0.98	1.64	1.88	1.18	3.66	1.34	0.96	0.62	1.00	1.28	2.34
Chester Bluff	1.07	1.92	1.26	2.42	1.34	1.67	1.67	1.48	1.30	1.45	1.31	0.49	1.98	1.41	1.80	2.37	3.60	2.38
Mile 293	2.51	1.55	0.99	1.18	1.74	0.44	0.51	1.27	2.12	0.68	2.38	2.61	1.62	1.22	2.48	2.58	2.96	3.00
Mirror Creek	2.56	1.54	1.02	2.00	1.97	0.57	0.60	2.08	1.95	1.05	2.81	1.69	1.67	1.45	2.40	3.75	3.13	2.85
Thistle (UT1805)	1.01	2.09	1.79	1.37	0.83	3.09	1.93	1.13	0.99	1.68	0.60	2.60	1.17	0.73	1.24	0.69	1.74	1.57
Thistle (UT1816)	0.63	2.45	1.72	1.04	0.81	1.78	0.78	0.55	0.35	1.35	0.52	3.34	0.71	0.42	0.41	0.67	0.83	1.70
Thistle (UT1823)	1.17	1.93	1.34	2.76	2.50	1.44	1.12	1.52	1.02	1.21	1.90	0.66	1.33	1.33	2.42	3.47	3.33	1.94
Caribou Ck 1	0.87	2.11	1.45	2.27	1.01	2.37	1.68	1.28	1.06	1.81	0.95	0.84	1.70	1.23	1.56	1.87	3.15	2.12
Caribou Ck 2	0.83	2.16	1.75	1.68	0.73	2.73	1.76	1.15	0.61	1.84	0.52	2.28	1.02	0.72	0.88	1.11	1.84	1.21
Klondike	1.95	1.97	1.34	3.23	2.26	2.24	2.04	2.87	2.09	2.22	2.52	1.09	2.93	2.09	2.49	4.49	5.79	4.11
Old Crow Basin	2.26	2.88	3.05	1.58	1.74	4.28	3.13	1.78	2.20	3.03	1.13	7.09	1.44	1.27	1.10	0.50	1.19	2.08
Dawson	53.98	45.13	41.16	50.54	50.90	42.48	44.62	54.60	56.32	45.19	56.11	46.66	50.34	50.29	49.93	59.64	61.13	65.29
DL	80.25	60.13	62.42	79.33	79.16	63.30	60.86	83.29	102.09	73.88	86.56	68.78	75.47	78.38	89.31	96.64	100.15	140.03
Togiak	41.14	25.34	26.47	33.32	35.80	29.39	27.74	34.94	42.88	30.19	38.42	35.30	31.02	32.86	36.74	40.74	38.49	45.33
C2 pumice 1	78.50	64.95	59.12	77.13	86.48	67.66	73.36	86.49	87.05	70.06	84.52	72.27	70.65	73.23	84.75	95.24	87.92	108.58
C2 pumice 2	93.89	68.18	66.78	92.02	106.43	82.25	89.44	102.41	107.50	86.02	99.68	86.79	80.51	86.64	109.03	115.30	103.84	138.99
C2 pumice 3	65.71	55.98	51.86	62.35	72.74	59.08	63.46	68.38	63.52	56.81	68.10	66.18	54.60	57.99	67.40	76.22	61.04	74.87

Birch Creek	Chester Bluff	Mile 293	Mirror Creek	UT1805 (Thistle)	UT1816 (Thistle)	UT1823 (Thistle)	Caribou Ck. 1	Caribou Ck. 2	Klondike	Old Crow Basin	Dawson	DL	Togiak	C2 pumice 1	C2 pumice 2	C2 pumice 3		
0.00																		
2.66	0.00																	
1.91	2.24	0.00																
1.73	2.12	0.96	0.00															
2.10	1.02	2.74	3.37	0.00														
0.69	2.23	2.12	2.24	1.20	0.00													
2.86	0.77	2.34	1.48	2.22	2.19	0.00												
2.13	0.19	2.79	2.23	0.75	1.70	0.70	0.00											
1.67	1.05	2.86	2.74	0.59	1.01	1.52	0.59	0.00										
3.52	0.43	3.94	2.23	2.49	3.37	1.39	0.52	1.87	0.00									
1.81	3.13	4.27	5.72	1.05	1.58	4.58	2.60	1.31	6.85	0.00								
52.07	36.20	43.97	42.53	56.02	57.27	46.82	43.82	52.80	49.99	67.73	0.00							
81.38	38.79	74.67	71.56	96.36	91.24	58.32	65.49	68.13	96.66	124.02	10.09	0.00						
36.20	27.70	24.40	23.78	48.30	40.11	32.85	37.41	35.73	43.43	44.20	22.52	37.89	0.00					
77.37	49.77	73.35	72.21	77.26	91.40	69.91	57.46	75.53	92.69	116.28	0.39	12.74	34.55	0.00				
93.55	54.34	91.20	91.63	93.42	110.92	82.15	63.71	84.56	130.02	144.42	0.72	11.48	38.97	2.72	0.00			
65.32	54.57	58.61	58.16	64.68	71.60	62.12	53.37	64.81	75.46	83.57	14.17	28.32	23.01	16.21	18.32	0.00		

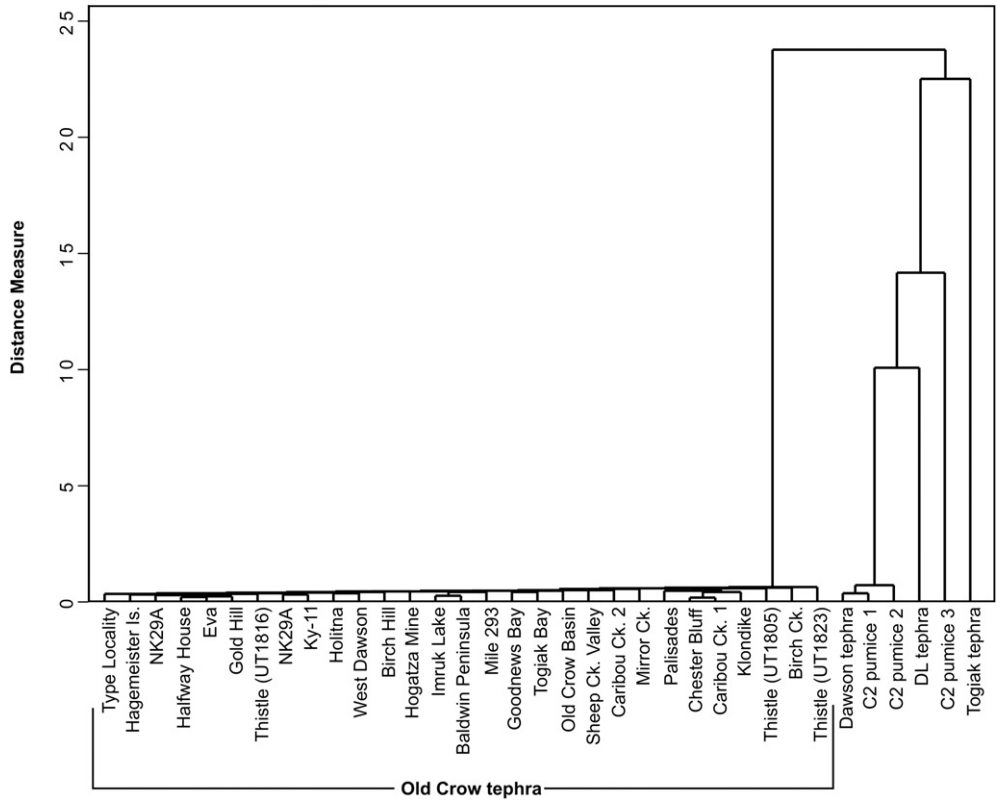

Fig. 12. Single-linkage cluster analysis performed on the matrix generated using the statistical distance measure of Perkins et al. (1995, 1998), calculated from 9 major-elements (glass shards). Note that all OCt samples group together at low joining distances forming one cluster which is separate from the clusters formed by Dawson, DL, Togiak, and C2 pumice 1, 2, and 3.

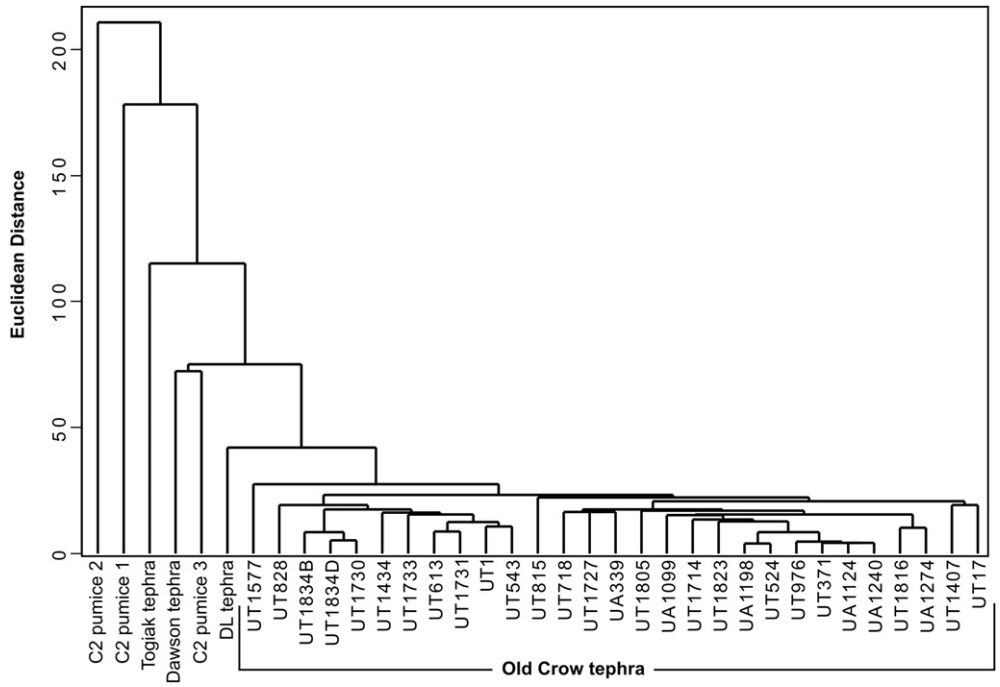

Fig. 13. Single-linkage cluster analysis performed on the Euclidean distance matrix generated from the trace-element composition of glass shards. Note that all OCt samples are grouped closely to each other with the compositionally similar tephra deposits Dawson, DL, Togiak, and C2 pumice 1, 2, and 3 joining at larger distances.

Table 10
Comparison of glass fission-track ages using the old and new calibration schemes.

Sample	Material	FT method	Glass FT age (±σ Ma)		Other dating methods	References
			Old calibration	New calibration	(±1σ)	
Reference glasses						
Jankov Moldavite (Czech R.)	Tektite	DCFT ITPFT	15.10 ± 0.47 15.38 ± 0.52 (15.23 ± 0.35)	14.28 ± 0.44 14.56 ± 0.49 (14.41 ± 0.33)	14.34 ± 0.08 Ma[a]	Staudacher et al. (1982) Laurenzi et al. (2003, 2007)
Roccastrada R2V glass (Italy)	Obsidian	DCFT ITPFT	2.58 ± 0.09 2.50 ± 0.11 (2.55 ± 0.07)	2.44 ± 0.09 2.36 ± 0.10 (2.40 ± 0.07)	2.45 ± 0.04 Ma (±2σ)[a]	Laurenzi et al. (2007)
JAS-G1 glass (Japan)	Obsidian	ITPFT	1.01 ± 0.06	0.94 ± 0.07	0.947 ± 0.005 Ma (±2σ)[a]	Kitada and Wadatsumi (1995)
Huckleberry Ridge tephra (U.S.A.)	Glass shards	DCFT ITPFT	2.19 ± 0.19 2.06 ± 0.26 (2.14 ± 0.15)	2.07 ± 0.18 1.94 ± 0.24 (2.02 ± 0.14)	2.003 ± 0.014 Ma (±2σ)[a]	Gansecki et al. (1988)
Old Crow tephra						
UT1434	Glass shards	ITPFT	129 ± 14 ka	122 ± 14 ka	128 ± 22 ka (min)[b]	Berger et al. (1996)
UT613	Glass shards	ITPFT	146 ± 28 ka	138 ± 27 ka	144 ± 22 ka (max)[b]	
UT501	Glass shards	ITPFT	156 ± 45 ka	148 ± 43 ka	131 + 21/-13 ka (min)[c]	Auclair et al. (2007)
UT613	Glass shards	ITPFT	120 ± 23 ka (131 ± 11 ka)	113 ± 22 ka (124 ± 10 ka)	135 + 21/-13 ka (max)[c]	Péwé et al. (2009)

Notes: The population-subtraction FT method was used; see Westgate et al. (2007) for details of DCFT and ITPFT methods. In the old calibration, ages were calculated using $\lambda_D = 1.551 \times 10^{-10}\ yr^{-1}$ and a zeta value of 318 based on six irradiations at the McMaster Nuclear Reactor, Hamilton, Ontario, using the NIST SRM 612 glass dosimeter and the Moldavite tektite with an $^{40}Ar/^{39}Ar$ plateau age of 15.21 ± 0.15 Ma (Staudacher et al., 1982). The new calibration is based on an $^{40}Ar/^{39}Ar$ age of 14.34 ± 0.08 Ma (Laurenzi et al., 2003, 2007) for the Moldavite, giving a zeta value of 301. Weighted mean age and error are given in brackets. Mean age estimates using the new calibration are about 5% younger, that is, within the error due to counting statistics for most of the Pleistocene tephra beds.

[a] Ages determined by the $^{40}Ar/^{39}Ar$ method.
[b] Ages determined by the thermoluminescence method.
[c] Ages determined by the infrared stimulated luminescence method.

volcanic center (ELVC) (Figs. 1 and 14). The ELVC featured at least four major caldera-forming eruptions at ~ 420, 290, 235, and 27 ka (Mangan et al., 2009), and pyroclastic materials from the youngest of these eruptions, C2, are compositionally similar to OCt. In addition, the observation by Waythomas et al. (2000, 2002) that ~ 238 ka tephra deposits and welded tuff along the Leontovich River in the ELVC have Fe-Ti oxide compositions and trace-element contents of glass shards that are only slightly different from OCt lends further support for a genetic link between ELVC and OCt. The only known ELVC volcanic unit of OCt age is a dacitic welded tuff, the Gap welded tuff, which has $^{40}Ar/^{39}Ar$ age determinations of 123 and 121 ka (Mangan et al., 2009; Waythomas et al., 2006). In the light of this information, it is tempting to believe that OCt relates to this dacitic tuff and its associated deposits, but an assessment of any such correlation must await further compositional studies.

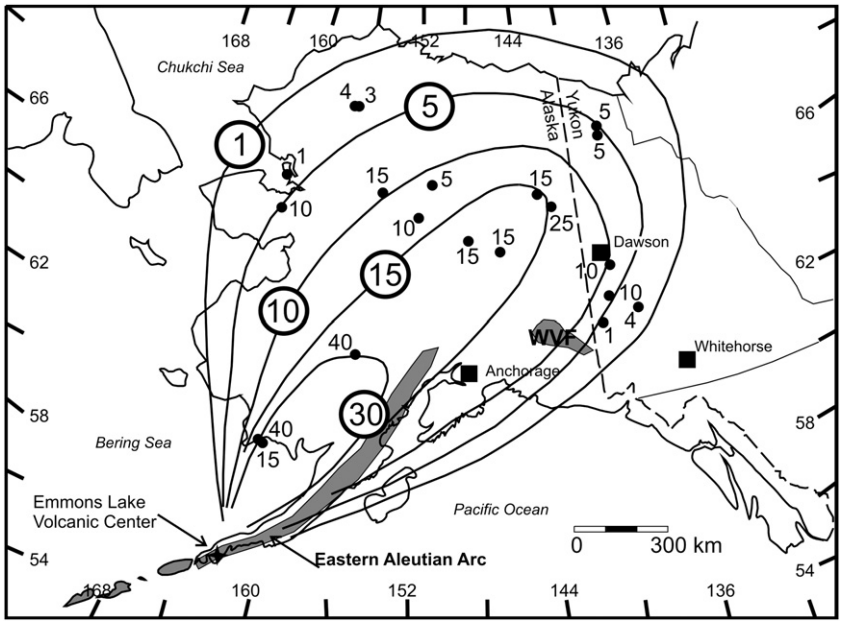

Fig. 14. Conservatively drawn isopachs across the Old Crow tephra fallout deposit. Thickness (in cm) of tephra bed at each site is noted. WVF is the Wrangell volcanic field.

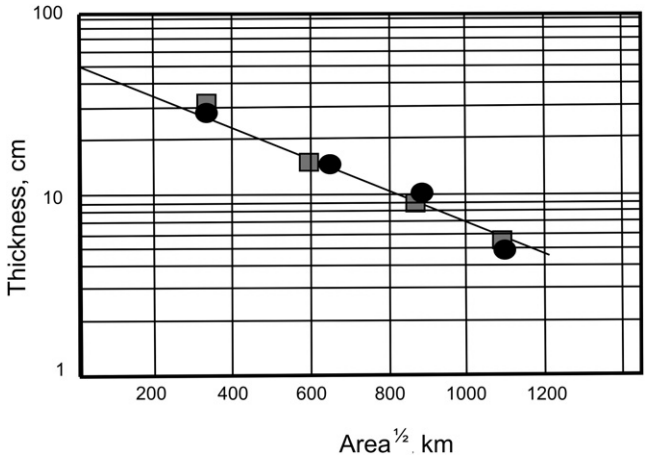

Fig. 15. Log of thickness versus the square root of area for Old Crow tephra with estimated straight line for calculating volume. Most distal isopach (1 cm) excluded. Squares indicate data derived from graphical method and circles are derived from the Garmin MapSource software.

Table 11
Comparison of area estimates within specified isopachs using two different methods.

Graphical Method			Garmin MapSource Software		
Thickness cm	Area within isopach km^2	Area $^{1/2}$ km^2	Thickness cm	Area within isopach km^2	Area $^{1/2}$ km^2
1	1,793,000	1339	1	1,726,696	1314
5	1,231,000	1110	5	1,193,280	1092
10	755,500	869	10	790,261	889
15	361,000	601	15	425,478	652
30	113,000	336	30	108,854	330

9. Conclusions

Stratigraphic and geochemical data indicate that Old Crow tephra is the result of a single, cataclysmic eruption. The proximal region may well have experienced tephra fallout from small eruptions just prior to or after the Old Crow event, but there is no evidence in the proximal region (or indeed in distal regions) that such small eruptions actually happened. A revised glass fission-track age for Old Crow tephra is 124 ± 10 ka. Stratigraphic and paleoecological contexts help to refine this age estimate in that they demonstrate deposition during latest MIS 6 time, that is, prior to growth of the last interglacial boreal forest in eastern Beringia. The bulk tephra volume is estimated by three different methods, which are in broad agreement at ~ 200 km^3, but this result must be considered as tentative given the poor controls on definition of isopachs over such a large area. The source caldera, although presently unrecognized, is located in the eastern Aleutian Arc, possibly at or near the Emmons Lake volcanic center.

Acknowledgements

Westgate and Froese acknowledge the support of the Natural Sciences and Engineering Research Council of Canada and the Yukon Geological Survey. National Science Foundation grant OPP-0002362 to Scott Elias, Thomas Hamilton and Mary Edwards funded Preece's fieldwork at the Noatak and Eva sites during 2000 and provided funds for some of the EMPA presented in this paper. T. Hamilton, G. Berger, and N. Bigelow helped in the stratigraphic interpretation and sampling of OCt at these two localities. We also thank T. Péwé, D. Kaufman, W. Manley, J. Brigham-Grette, T. Hamilton, M. Edwards, J. Matthews, M. Milner, A. Reyes, P. Colinvaux, P. Lea and V. Rampton for providing us with additional OCt samples, including their stratigraphic context. The Wigger family kindly allowed us access to the important Eva site, near Fairbanks, Alaska. We thank Chris Waythomas (United States Geological Survey, Anchorage) and Phil Shane (University of Auckland, New Zealand) for their critical assessments, which significantly improved the manuscript. In addition, Andy Brown at Aberystwyth University is thanked for his help in the preparation of samples for trace-element analysis.

Appendix. Supplementary data

Supplementary data associated with this article can be found in the online version, at doi:10.1016/j.quascirev.2010.04.020.

References

Alloway, B.V., Larsen, G., Lowe, D.J., Shane, P.A.R., Westgate, J.A., 2007. Tephrochronology. In: Elias, S.A. (Ed.), Encyclopedia of Quaternary Science. Elsevier Press, pp. 2869–2898.
Auclair, M., Lamothe, M., Lagroix, F., Banerjee, S.K., 2007. Luminescence investigation of loess and tephra from Halfway House section, central Alaska. Quaternary Geochronology 2, 34–38.
Bacon, C.R., Hirschmann, M.M., 1988. Mg/Mn partitioning as a test for equilibrium between coexisting Fe–Ti oxides. American Mineralogist 73, 57–61.
Balestrieri, M.L., Bigazzi, G., Bouška, V., Labrin, E., Hadler Neto, J.C., Kitada, N., Osorio, A.M., Poupeau, G., Wadatsumi, K., Zuniga, A., 1998. Potential glass age standards for fission-track dating: an overview. In: Van den haute, P., De Corte, F. (Eds.), Advances in Fission-Track Geochronology. Kluwer Academic Publishers, pp. 287–304.
Begét, J., Edwards, M., Hopkins, D., Keskinen, M., Kukla, G., 1991. Old Crow tephra found at the Palisades of the Yukon, Alaska. Quaternary Research 35, 291–297.
Begét, J.E., Keskinen, M.J., 2003. Trace-element geochemistry of individual glass shards of the Old Crow tephra and the age of the Delta glaciation, central Alaska. Quaternary Research 60, 63–69.
Berger, G.W., 2003. Luminescence chronology of late Pleistocene loess-paleosol and tephra sequences near Fairbanks, Alaska. Quaternary Research 60, 70–83.
Berger, G.W., Péwé, T.L., Westgate, J.A., Preece, S.J., 1996. Age of Sheep Creek tephra (Pleistocene) in central Alaska from thermoluminescence dating of bracketing loess. Quaternary Research 45, 263–270.
Carmichael, I.S.E., 1967. The iron-titanium oxides of salic volcanic rocks and their associated ferromagnesian silicates. Contributions to Mineralogy and Petrology 14, 36–64.
Denton, J.S., Pearce, N.J.G., 2008. Comment on Vinther et al. "A synchronized dating of three Greenland ice cores throughout the Holocene", the Minoan tephra is not present in the 1642 B.C. layer of the GRIP ice core. Journal of Geophysical Research 133, D04303. doi:10.1029/2007JD008970.
Elias, S.A., Hamilton, T.D., Edwards, M.E., Begét, J.E., Krumhardt, A.P., Lavoie, C., 1999. Late Pleistocene environments of the western Noatak basin, northwestern Alaska. Geological Society of America Bulletin 111, 769–789.
Fierstein, J., Nathenson, M., 1992. Another look at the calculation of fallout tephra volumes. Bulletin of Volcanology 54, 156–167.
Froese, D.G., Jensen, B.J., 2005. Stop 2: White River Ash-eastern lobe. In: Froese, D.G., Westgate, J.A., Alloway, B.V. (Eds.), Field Trip Guide for the International Field Conference and Workshop on Tephrochronology and Volcanism, Dawson City, Yukon Territory, Canada. Institute of Geological and Nuclear Sciences, New Zealand, pp. 53–56. Science Report 2005/26.
Froggatt, P.C., 1982. Review of methods of estimating rhyolitic tephra volumes; applications to the Taupo volcanic zone, New Zealand. Journal of Volcanology and Geothermal Research 14, 301–318.
Gansecki, C.A., Mahood, G.A., McWilliams, M., 1988. New ages for the climactic eruptions at Yellowstone: single-crystal ^{40}Ar/^{39}Ar dating identifies contamination. Geology 26, 343–346.
Ghiorso, M.S., Evans, B.W., 2008. Thermodynamics of rhombohedral oxide solid solutions and a revision of the Fe-Ti two-oxide geothermometer and oxygen-barometer. American Journal of Science 308, 957–1039.
Hamilton, T.D., Brigham-Grette, J., 1991. The last interglaciation in Alaska: stratigraphy and paleoecology of potential sites. Quaternary International 10-12, 49–71.
Jensen, B.J.L., Froese, D.G., Preece, S.J., Westgate, J.A., Stachel, T., 2008. An extensive middle to late Pleistocene tephrochronologic record from east-central Alaska. Quaternary Science Reviews 27, 411–427.
Kaufman, D.S., Manley, W.F., Forman, S.L., Layer, P.W., 2001a. Pre-late-Wisconsin glacial history, coastal Ahklun Mountains, southwestern Alaska – new amino acid, thermoluminescence, and ^{40}Ar/^{39}Ar results. Quaternary Science Reviews 20, 337–352.

Kaufman, D.S., Manley, W.F., Wolfe, A.P., Hu, F.S., Preece, S.J., Westgate, J.A., Forman, S.L., 2001b. The last interglacial to glacial transition, Togiak Bay, southwestern Alaska. Quaternary Research 55, 190–202.

Kitada, N., Wadatsumi, K., 1995. Proposal for a glass age standard "JAS-G1". Bulletin of Liaison and Informations, IUGS. Subcommission on Geochronology 13, 23–27.

Laurenzi, M.A., Bigazzi, G., Balestrieri, M.L., Bouška, V., 2003. $^{40}Ar/^{39}Ar$ laser probe dating of the central European tektite-producing impact event. Meteoritics and Planetary Science 38, 887–893.

Laurenzi, M.A., Balestrieri, M.L., Bigazzi, G., Hadler Neto, J.C., Iunes, P.J., Norelli, P., Oddone, M., Osorio Araya, A.M., Viramonte, J.G., 2007. New constraints on ages of glasses proposed as reference materials for fission-track dating. Geostandards and Geoanalytical Research 31, 105–124.

Lerbekmo, J.F., Westgate, J.A., Smith, D.G.W., Denton, G.H., 1975. New data on the character and history of the White River volcanic eruption, Alaska. In: Suggate, R.P., Cresswell, M.M. (Eds.), Quaternary Studies. Royal Society of New Zealand, Wellington, pp. 203–209.

Mangan, M., Miller, T., Waythomas, C., Trusdell, F., Calvert, A., Layer, P., 2009. Diverse lavas from closely spaced volcanoes drawing from a common parent: Emmons Lake Volcanic Center, eastern Aluetian Arc. Earth and Planetary Science Letters 287, 363–372.

Mangan, M.T., Waythomas, C.F., Miller, T.P., Trusdell, F.A., 2003. Emmons Lake Volcanic Center, Alaska Peninsula: source of the late Wisconsin Dawson tephra, Yukon Territory, Canada. Canadian Journal of Earth Sciences 40, 925–936.

Matheus, P., Begét, J., Mason, O., Gelvin-Reymiller, C., 2003. Late Pliocene to late Pleistocene environments preserved at the Palisades site, central Yukon River, Alaska. Quaternary Research 60, 33–43.

Matthews Jr., J.V., Schweger, C.E., Janssens, J.A., 1990. The last (Koy-Yukon) interglaciation in the northern Yukon: evidence from Unit 4 at Ch'ijee's Bluff, Bluefish Basin. Geographie physique et Quaternaire 44, 341–362.

McDowell, P.F., Edwards, M.E., 2001. Evidence of Quaternary climatic variations in a sequence of loess and related deposits at Birch Creek, Alaska: implications for the Stage 5 climatic chronology. Quaternary Science Reviews 20, 63–76.

Muhs, D.R., Ager, T.A., Begét, J.E., 2001. Vegetation and paleoclimate of the last interglacial period, central Alaska. Quaternary Science Reviews 20, 41–61.

O'Hara, M.J., Mathews, R.E., 1981. Geochemical evolution in an advancing, periodically replenished, periodically tapped, continuously fractionated magma chamber. Journal of the Geological Society of London 138, 237–277.

Pearce, N.J.G., Eastwood, W.J., Westgate, J.A., Perkins, W.T., 2002. Trace element composition of single glass shards in distal Minoan tephra from SW Turkey. Journal of the Geological Society of London 159, 545–556.

Pearce, N.J.G., Westgate, J.A., Perkins, W.T., Preece, S.J., 2004. The application of ICP-MS methods to tephrochronological problems. Applied Geochemistry 19, 289–322.

Pearce, N.J.G., Denton, J.S., Perkins, W.T., Westgate, J.A., Alloway, B.V., 2007. Correlation and characterization of individual glass shards from tephra deposits using trace element laser ablation ICP-MS analyses: current status and future potential. Journal of Quaternary Science 22, 721–736.

Pearce, N.J.G., Alloway, B.V., Westgate, J.A., 2008. Mid-Pleistocene silicic tephra beds in the Auckland region, New Zealand: their correlation and origins based on the trace element analyses of single glass shards. Quaternary International 178, 16–43.

Perkins, M.E., Brown, F.H., Nash, W.P., McIntosh, W., Williams, S.K., 1998. Sequence, age, and source of silicic fallout tuffs in middle to late Miocene basins of the northern Basin and Range province. Geological Society of America Bulletin 110, 344–360.

Perkins, M.E., Nash, W.P., Brown, F.H., Fleck, R.J., 1995. Fallout tuffs of Trapper Creek, Idaho – a record of Miocene explosive volcanism in the Snake River Plain volcanic province. Geological Society of America Bulletin 107, 1484–1506.

Péwé, T.L., Reger, R.D., 1983. Guidebook to permafrost and Quaternary geology along the Richardson and Glenn Highways between Fairbanks and Anchorage, Alaska. In: 4th International Conference on Permafrost, Alaska Division of Geological and Geophysical Surveys, Guidebook, vol. 1, 263 p.

Péwé, T.L., Berger, G.W., Westgate, J.A., Brown, P.M., Leavitt, S.W., 1997. Eva interglaciation forest bed, unglaciated east-central Alaska: global warming 125,000 years ago. Geological Society of America Special Paper 319, 54 p.

Péwé, T.L., Westgate, J.A., Preece, S.J., Brown, P.M., Leavitt, S.W., 2009. Late Pliocene Dawson Cut Forest Bed and new tephrochronological findings in the Gold Hill Loess, east-central Alaska. Geological Society of America Bulletin 121, 294–320.

Preece, S.J., Westgate, J.A., Gorton, M.P., 1992. Compositional variation and provenance of late Cenozoic distal tephra beds, Fairbanks area. Alaska. Quaternary International 13/14, 97–101.

Preece, S.J., Westgate, J.A., Stemper, B.A., Péwé, T.L., 1999. Tephrochronology of late Cenozoic loess at Fairbanks, central Alaska. Geological Society of America Bulletin 111, 71–90.

Preece, S.J., Westgate, J.A., Alloway, B.V., Milner, M.W., 2000. Characterization, identity, distribution, and source of late Cenozoic tephra beds in the Klondike district of the Yukon, Canada. Canadian Journal of Earth Sciences 37, 983–996.

Pyle, D.M., 1989. The thickness, volume and grainsize of tephra fall deposits. Bulletin of Volcanology 51, 1–15.

Reyes, A.V., Jensen, B.J.L., Zazula, G.D., Ager, T.A., Kuzmina, S., La Farge, C., Froese, D.G., 2010. A late-Middle Pleistocene (Marine Isotope Stage 6) vegetated surface buried by Old Crow tephra at the Palisades, interior Alaska. Quaternary Science Reviews 29, 801–811.

Richter, D.H., Preece, S.J., McGimsey, R.G., Westgate, J.A., 1995. Mount Churchill, Alaska: source of the late Holocene White River Ash. Canadian Journal of Earth Sciences 32, 741–748.

Rollinson, H.R., 1993. Using Geochemical Data: Evaluation, Presentation, Interpretation. Longman Scientific and Technical, Harlow, Essex, U.K., 352 p.

Schweger, C.E., Matthews Jr., J.V., 1985. Early and middle Wisconsinan environments of eastern Beringia: stratigraphic and paleoecological implications of the Old Crow tephra. Géographie physique et Quaternaire 39, 275–290.

Shane, P., 1998. Correlation of rhyolitic pyroclastic eruptive units from the Taupo volcanic zone by Fe–Ti oxide compositional data. Bulletin of Volcanology 60, 224–238.

Smith, V.C., Shane, P., Nairn, I.A., 2005. Trends in rhyolite geochemistry, mineralogy, and magma storage during the last 50 kyr at Okataina and Taupo volcanic centres, Taupo Volcanic Zone, New Zealand. Journal of Volcanology and Geothermal Research 148, 372–406.

Staudacher, T., Jessberger, E.K., Dominik, B., Kirsten, T., Schaeffer, O.A., 1982. $^{40}Ar/^{39}Ar$ ages of rocks and glasses from the Nördlinger Ries crater and the temperature history of impact breccias. Journal of Geophysics 51, 1–11.

Sun, S.-s., McDonough, W.F., 1989. Chemical and isotopic systematics of oceanic basalts: implications for mantle composition and processes. In: Saunders, A.D., Norry, M.J. (Eds.), Magmatism in the Ocean Basins. Geological Society Special Publication, No. 42, pp. 313–345.

Ward, B.C., Bond, J.D., Froese, D.G., Jensen, B., 2008. Old Crow tephra (140 ± 10 ka) constrains penultimate Reid glaciation in central Yukon Territory. Quaternary Science Reviews 27, 1909–1915.

Waythomas, C.F., Lea, P.D., Walter, R.C., 1993. Stratigraphic context of Old Crow tephra, Holitna Lowland, interior southwest Alaska. Quaternary Research 40, 20–29.

Waythomas, C.F., Miller, T.P., Mangan, M.T., Trusdell, F.A., 2000. Fire and ice on the Alaska Peninsula—stratigraphic records of pyroclastic eruptions and glaciations, Emmons Lake caldera and vicinity, southwestern Alaska. Eos Transactions of the American Geophysical Union 81 (48), F1352. Fall Meeting Supplement, Abstract 21B-05.

Waythomas, C.F., Miller, T.P., Mangan, M.T., Layer, P.W., Truesdell, F.A., 2002. Unique stratigraphic records of explosive volcanism and Quaternary glaciation, Emmons Lake caldera and vicinity, southwestern Alaska. Geological Society of America, Abstracts with Programs 34 (6), 549.

Waythomas, C.F., Miller, T.P., Mangan, M.T., 2006. Preliminary volcano hazard assessment for the Emmons Lake Volcanic Center, Alaska. United States Geological Survey Scientific Investigations Report 2006-5248, 33 p.

Westgate, J.A., Gorton, M.P., 1981. Correlation techniques in tephra studies. In: Self, S., Sparks, R.S.J. (Eds.), Tephra Studies. NATO Advanced Studies Institute Series. D. Reidel Publishing Company, pp. 73–94.

Westgate, J.A., Hamilton, T.D., Gorton, M.P., 1983. Old Crow tephra: a new late Pleistocene stratigraphic marker across north-central Alaska and western Yukon Territory. Quaternary Research 19, 38–54.

Westgate, J.A., Walter, R.C., Pearce, G.W., Gorton, M.P., 1985. Distribution, stratigraphy, petrochemistry, and palaeomagnetism of the late Pleistocene Old Crow tephra in Alaska and the Yukon. Canadian Journal of Earth Sciences 22, 893–906.

Westgate, J.A., 1988. Isothermal plateau fission-track age of the late Pleistocene Old Crow tephra, Alaska. Geophysical Research Letters 15, 376–379.

Westgate, J.A., Preece, S.J., Kotler, E., Hall, S., 2000. Dawson tephra: a prominent stratigraphic marker of late Wisconsinan age in west-central Yukon. Canadian Journal of Earth Sciences 37, 621–627.

Westgate, J.A., Naeser, N.D., Alloway, B.V., 2007. Fission-track dating. In: Elias, S. (Ed.), Encyclopedia of Quaternary Science. Elsevier Press, pp. 651–672.

Westgate, J.A., Preece, S.J., Froese, D.G., Pearce, N.J.G., Roberts, R.G., Demuro, M., Hart, W.K., Perkins, W.T., 2008. Changing ideas on the identity and stratigraphic significance of the Sheep Creek tephra beds in Alaska and the Yukon Territory, northwestern North America. Quaternary International 178, 183–209.

Westgate, J.A., Preece, S.J., Froese, D.G., Telka, A.M., Storer, J.E., Pearce, N.J.G., Enkin, R.J., Jackson, L.E., LeBarge, W., Perkins, W.T., 2009. Gold Run tephra: a middle Pleistocene stratigraphic and paleoenvironmental marker across west-central Yukon Territory, Canada. Canadian Journal of Earth Sciences 46, 465–478.